a Coriolis tutorial, Part 3:

β-effects; westward propagation

James F. Price

Woods Hole Oceanographic Institution,
Woods Hole, Massachusetts, 02543
https://www2.whoi.edu/staff/jprice/ jprice@whoi.edu

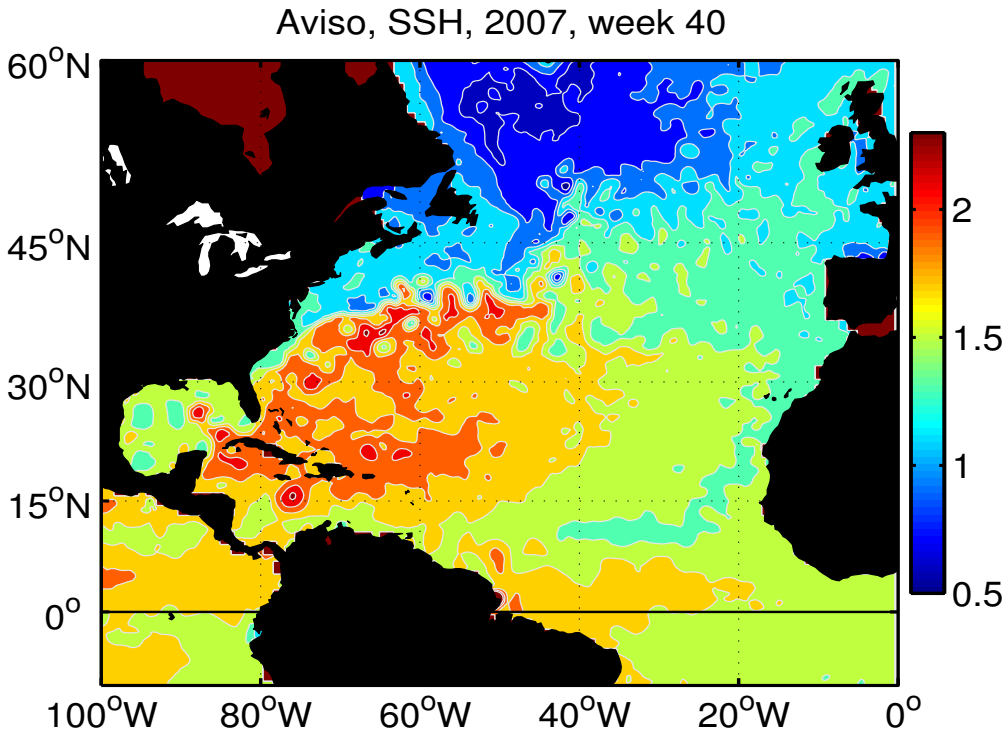

Figure 1: Sea surface height (SSH) over the North Atlantic observed by satellite altimetry. SSH variability occurs primarily on two spatial scales — basin scale gyres (thousands of kilometers), an SSH high in the subtropics and a low in the subpolar basin — and mesoscale eddies (several hundred kilometers) that are both highs and lows of SSH. The basin scale gyres are clearly present instantaneously, as here, and on long term time average, while mesoscale eddies are significantly time-dependent, including marked westward propagation. To see an animation, https://www2.whoi.edu/staff/jprice/Aviso-NA2007/ The goal of this essay is to learn how the northward increase of the Coriolis parameter leads to a westward propagation tendency for most large scale, low frequency phenomena, including the gyres and mesoscale eddies seen here.

Abstract: This is the third of a five-part introduction to the effects of Earth's rotation on the fluid dynamics of the atmosphere and ocean. The goal is to understand some of the very important beta effects (β-effects) that follow from the northward increase of the Coriolis parameter, f(latitude). The first problem considered is mid-latitude geostrophic adjustment configured as in Part 2 but with f represented by the linear approximation, $f = f_o + \beta y$, often called a β-plane. The short term (less than one week) adjustment is much the same as found on an f-plane, *viz*, spreading inertia-gravity waves that leave behind a nearly geostrophic eddy. On an f-plane, such an eddy could be exactly steady (absent diffusion or friction). On a β-plane, the same eddy will spontaneously translate westward at a slow and almost steady rate, about 3 km per day at 30^o latitude (south or north) and given scales that are typical of oceanic mesoscale eddies. This westward eddy translation has a great deal in common with the propagation of an elementary, long Rossby wave, and it is also consistent with the observed propagation of oceanic mesoscale eddies.

A similar adjustment experiment set in an equatorial region gives quite different results. Even fairly large, unbalanced thickness anomalies are rapidly dispersed into east and west-going waves. The west-going waves include the equivalent of inertia-gravity and Rossby waves. Long equatorial Rossby waves are nondispersive and have a phase and group speed of about 100 km per day, or 30 times the mid-latitude Rossby wave speed. The east-going Kelvin wave is still more impressive, as it carries the majority of the thickness anomaly in a single, nondispersive pulse that propagates eastward at the gravity wave speed, 300 km per day. Kelvin waves may thus transmit signals (say, an anomaly of upper ocean thickness) from mid-ocean to the eastern boundary within about a month.

These and other low frequency phenomenon are often interpreted most fruitfully as an aspect of potential vorticity conservation, the geophysical fluid equivalent of angular momentum conservation. Earth's rotation contributes planetary vorticity, f, that is generally considerably larger than the relative vorticity of winds and currents. Small changes in the latitude of a fluid column may convert planetary vorticity to a significant change of relative vorticity, or, if the horizontal scale of the motion is large compared to the radius of deformation, to a change in layer thickness (vortex stretching). The latter is the principal mechanism of westward propagation of long Rossby waves and of mid-latitude mesoscale eddies.

More on Figure 1: A one week average of SSH over the North Atlantic. This SSH is with respect to a level surface, with tides and high frequency variability removed. The color bar at right is in meters. These data were compiled and analyzed by the Aviso Project, https://www.aviso.altimetry.fr/ A slowly-varying, tilted SSH implies a near-surface geostrophic current that is approximately parallel to isolines of SSH. Along with geostrophic currents, there may also be wind-driven Ekman currents that are not directly visible here. Compared with the year-long mean of Fig. 1, Part 1, this field shows considerable variability on scales of several hundred kilometers, often termed the oceanic mesoscale and emphasized in this essay.

Contents

1 Large-scale flows of the atmosphere and ocean are markedly anisotropic

A thorough-going understanding (intuition) of the Coriolis force and geostrophy are a good starting point for a study of the atmosphere and ocean. However, geostrophy is nowhere near the end of the road: an exact geostrophic balance, i.e., geostrophy on an f-plane as used in Part 2, implies exactly steady winds and currents that never evolve. Moreover, f-plane phenomena are intrinsically isotropic, showing no favored direction. In sharp contrast to these properties of an f-plane model, observations from the atmosphere and the ocean show that nearly all large scale winds and currents evolve slowly but continually, even absent external forcing, and that they often exhibit a marked east-west anisotropy of one or more properties. Three important examples of this east-west asymmetry evident in Fig. 1 are:

1.1 Mesoscale Eddies

The SSH data of Fig. 1 (and especially its animation linked in the caption) reveal a number of important, characteristic properties of the mesoscale eddy field:

1. **Space and time scales.** Any given snapshot of SSH will reveal variability in the form of more or less round SSH anomalies having a radius $L \approx 200$ km, an SSH amplitude of typically $\pm$ 0.1 m and currents $U \approx 0.1$ m sec^{-1} — mesoscale eddies. Direct measurements of ocean currents within eddies indicate that their momentum balance is close to being geostrophic, as we would have expected given their modest amplitude and typically small Rossby number, $R_o \leq 0.05$ (Sec. 5, Part 2). A given eddy, i.e., a specific SSH anomaly, can often be identified and tracked for many months. Highs and lows of SSH — anti-cyclones and cyclones — are about equally common.

2. **Westward propagation.** Aside from regions having strong mean currents, e.g., the North Brazil current or the Gulf Stream and its extension into the subpolar gyre, mesoscale eddies propagate westward, slowly, but relentlessly. On average over all ocean basins, the eddy propagation speed at 30 deg latitude has been estimated from satellite altimetric data to be $3.5 \pm 1.5 \times 10^{-2}$ m sec^{-1} or about 3 km day^{-1}. The observed eddy propagation speed decreases somewhat toward higher latitude, and increases markedly toward lower latitudes down to about 15 deg. At still lower latitudes, the SSH signature of mesoscale eddies is much reduced.[1]

3. **Geography and seasonality.** Mesoscale eddies are very widespread but their amplitude shows considerable spatial variability. The largest SSH amplitudes, up to about about ± 0.2 m, are found near the western boundaries of the subtropical and subpolar basins. Eddy amplitudes are considerably less in the eastern half of the subtropical North Atlantic, and mesoscale eddies are less common in the equatorial region, outside of the North Brazil current. There is very little evidence of seasonality of eddy amplitude or other properties, suggesting that direct forcing by the atmosphere is not the primary generation process (the equatorial region again being a partial exception).

1.2 Other phenomena

1.2.1 Equatorial variability

SSH variability seen in the equatorial region ($\pm 10^o$ of the equator) is quite different from that seen at higher latitudes. Mesoscale eddies are, by comparison with higher latitudes, uncommon. SSH variability occurs primarily in zonally elongated and meridionally compressed features that are displaced from the equator by 5 to 10^o and that appear to have significant seasonality. There are occasional events of rapid eastward propagation along the equator, several hundred kilometers per day, sometimes spanning almost the entire basin.

[1] A comprehensive analysis of mesoscale eddies observed in altimetric data is by Chelton, D.B., Schlax, M.G., Samelson, R.M.,2011, Global Observations of Nonlinear Mesoscale Eddies, *Progress in Oceanography*, doi: 10.1016/j.pocean.2011.01.002. Other recent analyses of the oceanic mesoscale are by Fu, L., D. B. Chelton, P. Le Traon and R. Morrow, 'Eddy dynamics from satellite altimetry', *Oceanography Mag.*, 2010, and by Zang, X. and C. Wunsch, 1999, *J. Phys. Oceanogr.*, 29, 2183-2199. Fu, L-L., 2009, 'Pattern and velocity propagation of the global ocean eddy variability', *J. Geophys-Res Oceans*, 114, C11017, doi:10.1029/2009JC005349 describes the often very large effect of the time-mean ocean circulation upon eddy propagation.

1.2.2 Upper Ocean Gyres

Fig. 1 is centered on the North Atlantic subtropical gyre, a high pressure (high SSH) clockwise rotating, basin-filling circulation that is driven by the overlying winds. A striking characteristic of all wind-driven ocean gyres is that they are strongly compressed onto the western side of the basin, often termed western intensification. This and other aspects of wind-driven circulation will be deferred to Part 4.

1.3 Goals and the plan of this essay

The goal of this essay is to take a significant step beyond f-plane geostrophy and address .... **What process(es) lead to the time-dependence and marked east-west asymmetry of most large-scale flow phenomena?** There are many processes that can cause departures from geostrophy and time-dependence, including drag on an upper or lower boundary, which will be considered here in a simplified form. However, another process(es), called the β-effect(s), is the emphasis here. β-effects are ubiquitous in that they arise merely from north-south flow in combination with the northward increase of the Coriolis parameter,

$$f(\phi) = 2\Omega \sin(\phi), \tag{1}$$

where ϕ is the latitude. The $f(\phi)$ above can often be used as is, but for our purpose it is helpful to use the linear approximation that

$$f(y) = f(\phi_o) + \frac{df}{dy} y + HOT, \tag{2}$$

where $y = R_E(\phi - \phi_o)$ is the north-south (Cartesian) coordinate, R_E is Earth's nominal radius, approx. 6370 km. The coefficient of the linear term is very often written as

$$\boxed{\beta = \frac{df}{dy} = \frac{2\Omega}{R_E}\cos\phi_0} \tag{3}$$

When the higher order terms (HOT) of (2) are ignored, the resulting linear model

$$\boxed{f(y) \;=\; f(\phi_o) \;+\; \beta y} \tag{4}$$

is often called a β-plane. β is positive in both hemispheres, has a maximum at the equator, and goes to zero at the poles. At 30^o N, say, $\beta = 2.29 \times 10^{-11}\mathrm{m}^{-1}\mathrm{s}^{-1}$, which looks to be very small. However, the appropriate comparison is βL with the constant term $f_o = f(\phi_o)$ of (2), where L is the horizontal scale of the motion, and then it is apparent that the β term is $\propto L/R_E$. The β term is still small for mesoscale-sized phenomena, $L = O(10^5)$ m. However, β effects may be systematic and persistent, and may thus become important over a long term, say months.

The plan is to solve and analyze a sequence of idealized adjustment experiments posed in a shallow water (single layer fluid) numerical model in which the Coriolis parameter is represented by the β-plane approximation, Eqn. (4). The shallow water momentum and continuity equations were written in Sec. 2, Part 2 and will not be repeated until some new terms are added in Part 4. The configuration is an open domain, very much like that of Part 2. Mid-latitude, mesoscale eddies are treated in Sec. 2, and a similar equatorial adjustment experiment is considered in Sec. 3.

The emphasis here is on β-effects rather then the shallow water model *per se* or its analysis, but there two aspects of the model and method that you should watch for. First, the shallow water equations solved here are nonlinear, in common with all but the most simplified fluid models. Whether the solution exhibits appreciable finite amplitude phenomena depends upon the amplitude of the initial eddy (Sec. 2) or wind stress (Part 4). Amplitudes are chosen to be realistic of the phenomena of Fig. 1, and as a result, finite amplitude effects are appreciable but generally not dominant. However, this depends very much on the specific phenomenon under consideration, i.e., whether eddy propagation, which looks to be nearly linear, or parcel displacement caused by the eddy, which is significantly nonlinear. Second, the primary analysis method is diagnosis of the potential vorticity balance, i.e. q-balance. This was very fruitful for understanding the geostrophic adjustment phenomena of Part 2, and it is almost indispensable for interpretation of the upcoming experiments. Gaining some fluency with the concepts of q-balance will be invaluable for your study of oceanic and atmospheric dynamics, and an implicit goal of this essay is to help you make a start.

1.4 Acknowledgments

Financial support during the preparation of these essays was provided by the Academic Programs Office of the Woods Hole Oceanographic Institution. Additional salary support has been provided by the U.S. Office of Naval Research.

2 Adjustment and propagation on a mid-latitude β-plane

We can begin to understand some of the observed properties noted in Sec. 1.1 by studying the evolution of a single eddy made by geostrophic adjustment, just as in Part 2, with the only new wrinkle being $f(\phi)$ given by Eqns. (3) and (4) vs. an f-plane in Part 2. As well, the integrations are continued for a much longer duration, up to a year. The spatial domain of the model is two-dimensional, with $(x,\ y)$ the east and north coordinates, and the domain is 3000 km on a side. The undisturbed layer thickness, H = 500 m. The initial condition is taken to be a right cylinder of radius $L = 100$ km, and thickness anomaly, $\eta_0 = 50$ m. This corresponds to an SSH anomaly of about 0.1 m (from the reduced gravity approximation, Sec. 2, Part 2), which is typical of observed SSH mesoscale variability. The initial velocity is everywhere at rest. The initial eddy is thus a potential vorticity anomaly compared to the outlying fluid, i.e., inside the initial eddy, $q = f/(\eta_0 + H)$, while outside, $q = f/H$. Everything that we saw and learned from the f-plane adjustment experiments in Part 2 will recur here, but alongside several new and very important phenomena — β-effects — that owe their existence to the inclusion of the β term in (2). There are two kinds of beta-effects noted here, high frequency beta effects upon inertia-gravity waves which is discussed very briefly, and low frequency beta effects that are the central topic.[2]

2.1 High frequency beta-effects on inertia-gravity wave propagation

In the case of a mesoscale eddy having radius $L = 100$ km, the spatial variation of f is small, $\beta\delta y/f_o = 2L/R_E \approx 0.03$, and so it is not surprising that the first few days of the geostrophic adjustment process are very similar to that seen in the f-plane experiments of Part 2, including, initially, isotropic radiation of inertia-gravity waves Fig. (2), and the animation linked in the caption. But after about a week, the inertia-gravity wave field develops a noticeable north-south asymmetry. The waves that propagate poleward (northward in this case) are propagating toward higher f. Within a few thousand kilometers these waves reach a latitude at which their intrinsic frequency approaches f. Recall from Part 2 that free inertia-gravity waves can not exist at a latitude where their frequency is less than the local inertial frequency, f, and this is true on a β-plane as well. Poleward-traveling inertia-gravity waves are thus reflected equatorward. After about ten days have passed, the region that is poleward (northward) of the eddy is nearly free of inertia-gravity waves, while the equatorward side is still fairly energetic. This β-induced refraction of inertia-gravity waves is an interesting and important process of the ocean's internal wave sea state. However, the emphasis here is on low frequency phenomenon, and this particular high-frequency β-effect will not be discussed in depth.

[2]These experiments start with a mesoscale eddy-sized q anomaly. This raises the important question — why are there such thickness anomalies in the first place? — considered very briefly in Sec. 2.5.

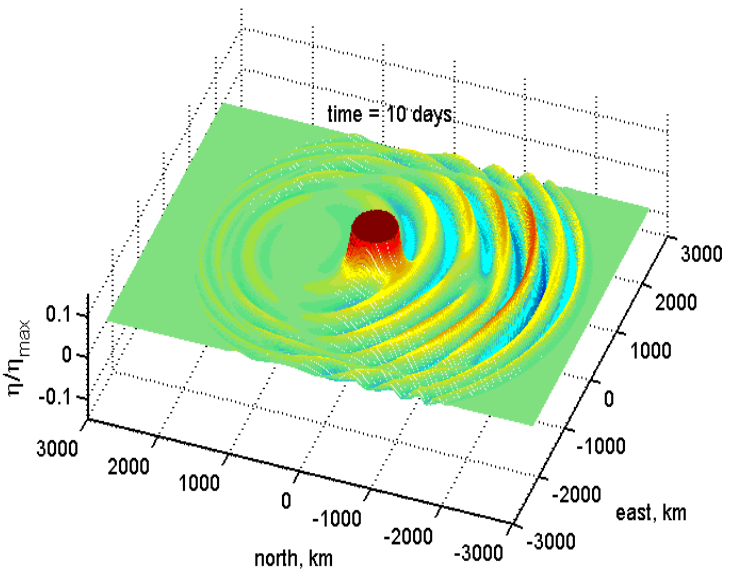

Figure 2: A snapshot of scaled thickness anomaly ($\eta_{max} = \eta_0 = 50$ m) 10 days after the start of a β-plane adjustment experiment. Poleward (north) is to the left in this figure. The vertical scale is severely truncated to emphasize the comparatively small amplitude inertia-gravity waves. By this time the wave amplitude is much reduced on the poleward side of the eddy. This north-south asymmetry in wave amplitude is due to a beta-induced reflection of the poleward-traveling, inertia-gravity waves. An animation of this data is igwaves-beta.mp4 in the P3 video collection https://www2.whoi.edu/staff/jprice/P3-videos

2.2 Low frequency beta-effect; westward propagation of nearly geostrophic eddies

Over a longer time, this experiment reveals a wholly new process that follows from the seemingly small change made to the Coriolis parameter — the eddy peak moves almost due westward at a slow but steady rate, -0.03 m sec^{-1} or roughly 3 km per day (Fig. 3). This westward propagation is significant in that it is 1) a robust and well-resolved feature of the numerical solution, and 2) closely comparable to the observed, westward propagation of ocean mesoscale eddies at this latitude (Fig. 1). Notice that the eddy peak just about keeps pace with the thin red line of Fig. (3) that is translated westward at the long Rossby wave speed appropriate to the present stratification and central latitude, $-\beta R_d^2 = -0.036$ m sec^{-1}, discussed in detail in Sec. 2.4.

The eddy peak in η remains well-defined, though the amplitude diminishes over time, especially at the beginning of the experiment. A spreading wake of decidedly wavy-looking ridges and troughs appears to trail behind the eddy peak, and eventually extends slightly eastward of the initial eastward edge, $x = 100$ km. The energy present in these waves must have come from the initial potential energy of the raised interface, and hence the spreading of energy away from the eddy peak is consistent with the decrease in the eddy peak amplitude.

The primary goals for the remainder of this section are to develop an understanding of the westward

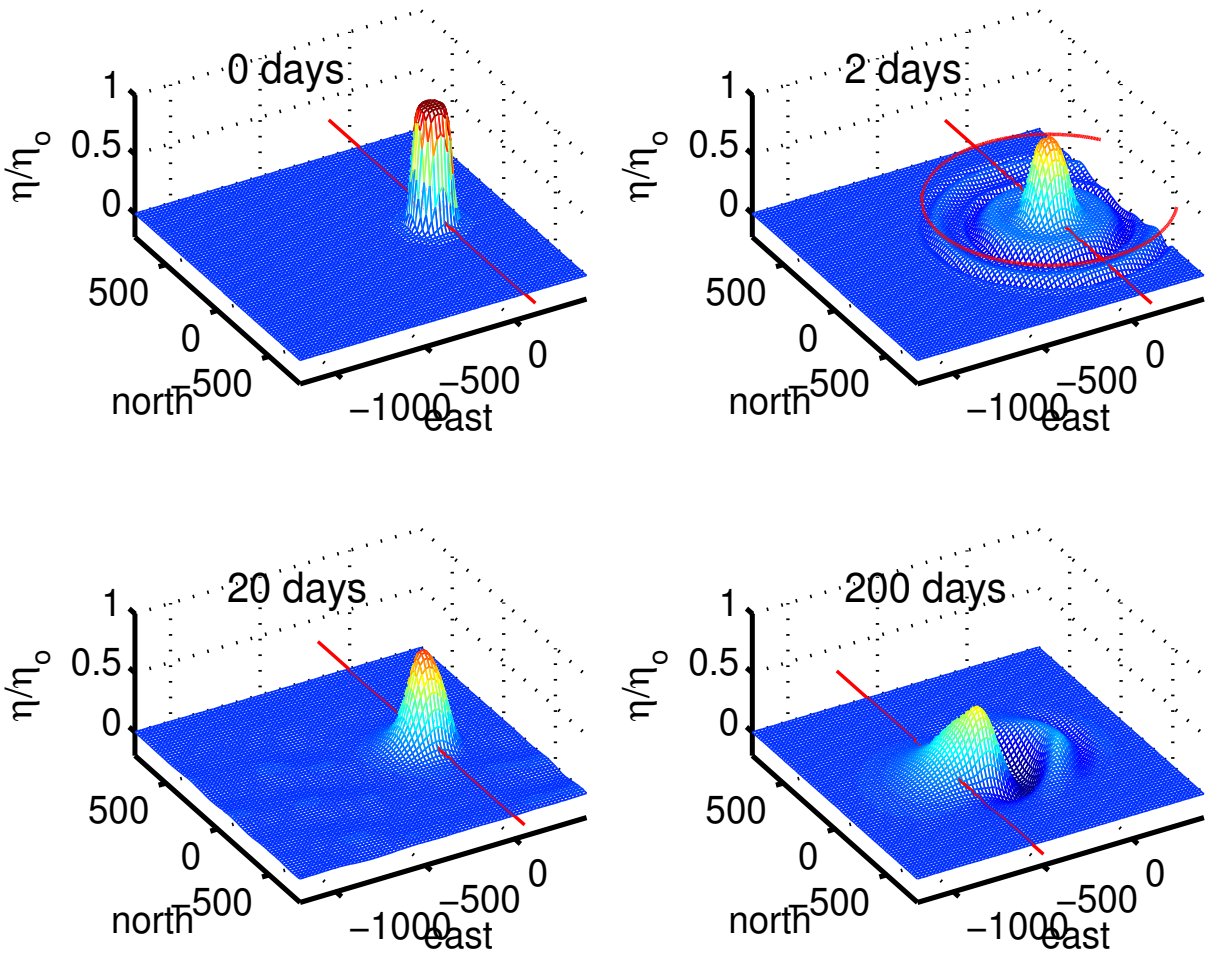

Figure 3: A numerical experiment in geostrophic adjustment on a β-plane solved by the numerical model geoadj_2d.for The normalized anomaly of layer thickness, η/η_0 ($\eta_o = 50$ m), is shown at four times: (upper left) the initial state of rest at $time = t = 0$, (upper right) 2 days after the eddy was released, and while inertia-gravity waves were prominent, (lower left) at 20 days, and (lower right) at 200 days, by which time the beta-induced westward propagation of the eddy peak is pronounced. The figures are annotated with a thin red circle having a radius $r = L + C\,t$ that expands at the gravity wave speed, $C = \sqrt{g'H} \approx 300$ km day^{-1} and so is off the model domain in about five days. There is also a thin red line oriented north-south that moves westward at the long Rossby wave speed, $-\beta R_d^2$, which is about 3 km day^{-1} for this experiment (Sec. 2.3). It can be very helpful to see these data animated, see pos50-h.mp4 in https://www2.whoi.edu/staff/jprice/P3-videos

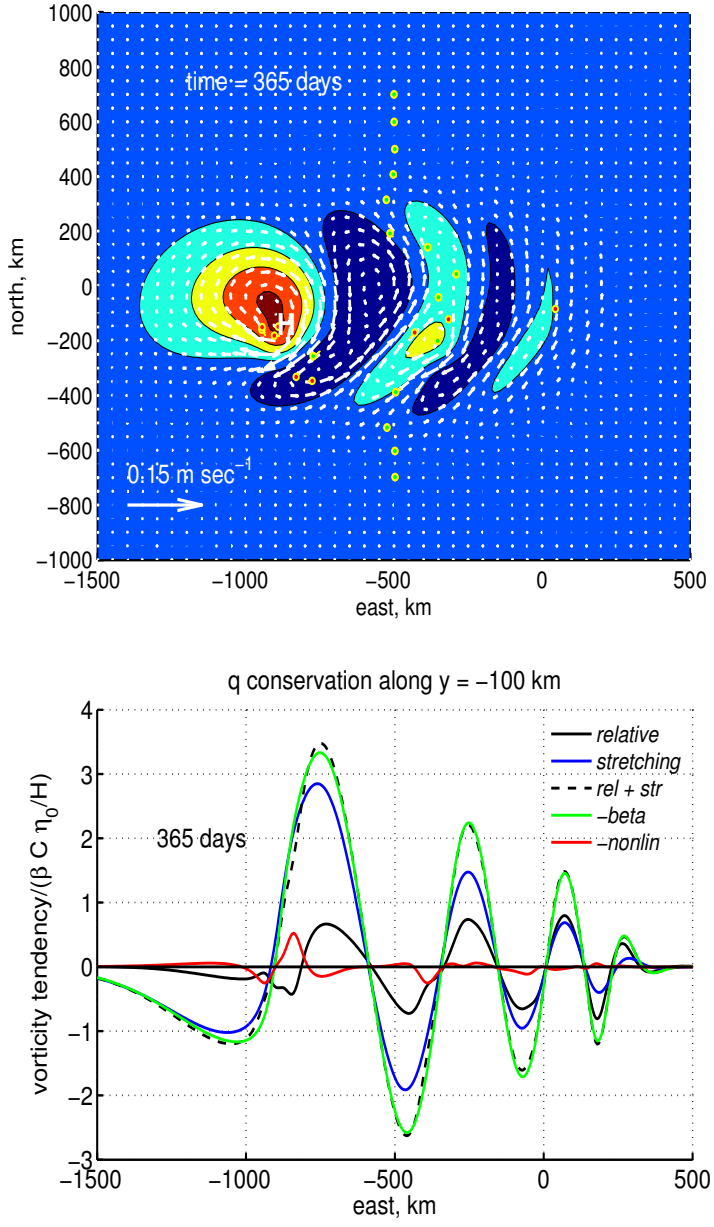

Figure 4: **(upper)** A snapshot of the horizontal velocity and thickness anomaly η (color contours, proportional to pressure) from the β-plane geostrophic adjustment experiment of Fig. (3). The north coordinate, y, was centered on 30^oN; the east coordinate, x, increases to the right. The big vector at lower left has a magnitude $0.5C\eta_0/H$ and serves as a scale for speed. This is a snapshot at 365 days; an animation is pos50-u.mp4 in the P3-videos collection. The red and green dots are floats (passive fluid parcels) that will be discussed in Sec. 2.5. **(lower)** The potential vorticity balance (8) evaluated at $time = 365$ days along the line $y = -100$ km through the eddy peak in η. Here the β term has been moved to the right side of the equation, as *relative + stretching = -beta - nonlin* which helps show that (negative) *beta* term (green line) is closely balanced by the sum of the time rate of change of *relative* vorticity (black line) and vortex *stretching* (blue line; the sum *relative + stretching* is the black dashed line). Notice that the horizontal scale of the motion decreases from west to east, while the ratio relative/stretching (black/blue) increases from west to east. This systematic variation of horizontal scale and q-conservation mechanism is characteristic of a dispersing Rossby wave pulse discussed in Sec. 2.3.

propagation of the eddy peak and the spreading (dispersion) of energy. The implicit assumption is that if we can understand these aspects of the numerical experiment, then we will have developed also a candidate understanding of the westward propagation of oceanic mesoscale eddies.[3]

The westward propagation of the eddy peak seen in Fig. (3) is reminiscent of the propagation of the wave pulses of Sec. 3 Part 2 insofar as the eddy peak propagates steadily and as a somewhat coherent feature (though with appreciable decay discussed below). This westward propagation is very slow, however, only about one percent of the gravity wave speed, C. At a fixed point, the time rate of change, and thus the frequency, ω, is correspondingly very low, about 1% of f. Is there a useful wave description of this westward propagation? The corresponding wave motion is certainly not contained within the f-plane model, since no free motion exists in the low frequency band $0 \leq \omega \leq f$ (Sec. 4, Part 2) and even more to the point, a balanced eddy stays where it is put on an f-plane (Sec. 5, Part 2). An analysis of westward propagation will evidently require taking explicit account of the one new feature of this experiment, the northward variation of f represented in Eqn. (2) by βy. The straightforward and appealing technique of looking for plane wave solutions directly in the governing equations (Sec. 4, Part 2) does not go through when $f = f(y)$ since the coefficients in the linear shallow water equations are then not constants.

How to proceed? Two clues: 1) In the shallow water model integrated here the potential vorticity should be conserved following parcels since there is no external forcing (and aside from real or inadvertent numerical diffusion). In that sense the conservation of potential vorticity is already known,

$$\frac{Dq}{Dt} = \frac{D}{Dt}\left(\frac{\xi + f}{h}\right) = 0. \tag{5}$$

It remains to learn how the various terms of (5) achieve this balance, and doing so yields considerable insight into the mechanism of westward propagation (Sec. 2.4). 2) The velocity and pressure fields associated with the propagating eddy are transverse and nearly geostrophic; it is hard to see any discrepancy between the velocity direction and the local pressure isolines, though exact geostrophic momentum balance clearly can not hold. Nevertheless, geostrophy might be used to eliminate one of η or ξ and so to arrive at a governing equation for the slowly evolving, nearly geostrophic flow seen in this experiment.

The shallow water q-conservation equation (5) expanded and noting that $h = H + \eta$ and

[3] Westward propagation persists until the eddy peak reaches the western boundary of the computational domain. The subsequent evolution of the eddy depends entirely upon the boundary condition imposed on the western edge of the domain. The radiation boundary condition used here (Sec. 2.2, Part 2), $\partial(\ )/\partial t = -U_{rad}\partial(\ )/\partial x$ with $U_{rad} = C = \sqrt{g'H} = 3$ m sec^{-1}, is effective at minimizing the undesirable reflection of the fast-moving gravity waves. However, this comparatively large U_{rad} will act to push the eddy through the western boundary much more rapidly than it would otherwise go. Since the gravity wave and Rossby wave processes are so distinct in this experiment, it is sufficient to simply reset U_{rad} to the long Rossby wave speed, $U_{rad} = \beta R_d^2 \approx 0.03$ m sec^{-1} (Sec. 2.2) after enough time has elapsed, 30 days.

$Df/Dt = \partial f/\partial t + v\partial f/\partial y = \beta v$ is

$$\frac{D\xi}{Dt} - \frac{D\eta}{Dt}\frac{\xi+f}{(H+\eta)} + \beta v = 0, \tag{6}$$

$$nonlin\ relative + nonlin\ stretching + beta = 0.$$

The terms are the material time rate change of *relative* vorticity, the material time rate change of thickness, here called vortex *stretching*, and the very important *beta* effect due to meridional flow through a y-varying f. Since this D/Dt is the material derivative, the first two terms are nonlinear. As we will see shortly, the dominant terms for this experiment are three linear terms that are embedded in (6), and it is very helpful to sort them out. The important *beta* term is linear as is. The *nonlin relative* term is easily factored into a local time rate of change, which is linear, and an advection term that is nonlinear,

$$\frac{D\xi}{Dt} = \frac{\partial\xi}{\partial t} + \mathbf{V}\cdot\nabla\xi.$$

The *nonlin stretching* term may be expanded into

$$\frac{D\eta}{Dt}\frac{\xi+f}{(H+\eta)} = \frac{\partial\eta}{\partial t}\frac{f}{H} - \frac{\partial\eta}{\partial t}\frac{\eta f}{(H+\eta)^2} + \frac{\partial\eta}{\partial t}\frac{\xi}{H+\eta} + \mathbf{V}\cdot\nabla\eta\frac{\xi+f}{H+\eta}, \tag{7}$$

where the first term on the right side of (7) is linear and usually the largest term, and the next three terms are all nonlinear. Substituting these expansions into (6) and collecting the linear terms on the left yields[4]

$$\frac{\partial\xi}{\partial t} - \frac{f}{H}\frac{\partial\eta}{\partial t} + \beta v = -\mathbf{V}\cdot\nabla\xi + \frac{\partial\eta}{\partial t}\frac{\eta f}{(H+\eta)^2} - \frac{\partial\eta}{\partial t}\frac{\xi}{H+\eta} - \mathbf{V}\cdot\nabla\eta\frac{\xi+f}{H+\eta}, \tag{8}$$

$$relative + stretching + beta = -nonlin.$$

The terms of Eqn. (8) evaluated along an east-west slice through the eddy peak η, along $y = -100$ km, and for the $time = 365$ days are in Fig. (4), bottom. The nonlinear term (red line) is appreciable near the eddy peak, but over most of the domain and including within the eddy, the β term is very nearly balanced by the sum of the relative and stretching vorticity terms, which are in phase. Thus the q balance of this phenomenon approximates the linear q balance,

$$\boxed{\frac{\partial\xi}{\partial t} - \frac{f}{H}\frac{\partial\eta}{\partial t} + \beta v = 0} \tag{9}$$

$$relative + stretching + beta = 0.$$

[4]Notice that the dimension of these terms is *vorticity time*$^{-1}$, i.e., it is a vorticity tendency equation. Eqn. (6) will nevertheless be referred to as a *potential* vorticity conservation equation, since that was the essential origin.

Many of the large scale, low frequency phenomena of the atmosphere and ocean have a significant overlap with this linear q-balance, even when, as here, they may also exhibit finite amplitude effects and be subject to external forcing. The upcoming Sec. 2.3 will examine the free waves that are supported by Eqn. (9), planetary Rossby waves, and finite amplitude (nonlinear) effects will be discussed in Sec. 2.4.

Assuming that the object will be motions having very low frequency, $\omega/f \ll 1$, and modest amplitudes, $\eta/H \ll 1$, then the velocity and pressure will be nearly geostrophic. In that case the geostrophic relations for north-south velocity, $v = (g'/f)\partial\eta/\partial x$, and vorticity, $\xi = (g'/f)\nabla^2\eta$, may be substituted in to Eqn. (9) to eliminate the velocity components in favor of η. After a little rearrangement there comes a linear, third order governing equation for η,

$$(\frac{g'H}{f^2}\nabla^2 \; - \; 1)\frac{\partial\eta}{\partial t} \; - \; \frac{\beta g'H}{f^2}\frac{\partial\eta}{\partial x} \; = \; 0, \tag{10}$$

$$relative + stretching + beta = 0.$$

Notice that the time derivative of η is proportional to the first derivative of η in one direction, east-west. The dynamics of a β-plane is evidently anisotropic (not the same in all directions), which is a significant difference from an f-plane. This crucial dependence upon direction can be attributed to Earth's rotation vector (Part 1), which defines a specific direction for geophysical flow phenomena that are 1) low frequency enough to be significantly effected by the Coriolis force and 2) that have sufficiently large horizontal scale to be effected by the spatial variation of f due to Earth's nearly spherical shape.

2.3 Planetary Rossby waves

It is of considerable interest to learn how the balance of potential vorticity depends upon the horizontal spatial scales and the time scale of the motion. To learn the result for the important case of linear and nearly geostrophic potential vorticity, Eqn. (10), we need only substitute an elementary plane wave form,

$$\eta(x,t) \; = \; \eta_0 \exp(i(k_x x + k_y y - \omega t)) \tag{11}$$

into Eqn. (10). A spatial derivative in the x direction thus brings out the east-west component of the wavenumber, k_x, and a partial time derivative brings out the frequency, ω (assumed to be positive in all that follows). Solving for ω yields the dispersion relation for planetary Rossby waves, [5] Fig. (5),

$$\boxed{\omega \; = \; -\beta R_d \left(\frac{R_d k_x}{1 + R_d^2(k_x^2 + k_y^2)} \right)} \tag{12}$$

[5]The terms 'eddy' and 'wave' are widely used, sometimes almost interchangeably. In fluid mechanics parlance, the most general use of 'eddy' is to denote any kind of departure from a spatial or a temporal mean. Here, eddy will be used to denote a flow feature having a quasi-circular planform and a thus more or less closed circulation. Mesoscale eddies are an example, and of course they are also a departure (anomaly) from a time or space average that would be appropriate for defining a basin-scale

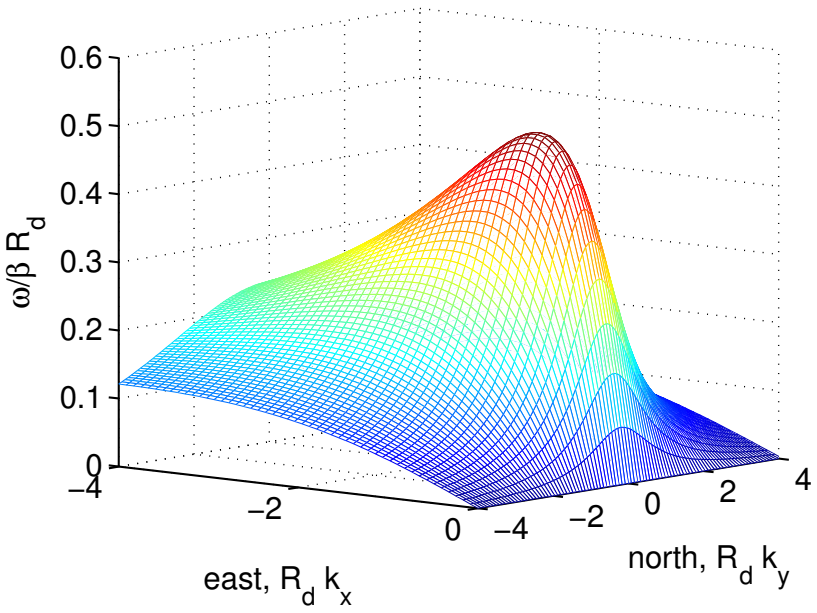

Figure 5: The dispersion relation for planetary Rossby waves, Eqn. (12). Frequency is normalized by $\beta R_d = 2\pi/85$ days, evaluated for a baroclinic midlatitude ocean. This surface is symmetric in the north-south component of the wavenumber vector, k_y. The east-west component can only be negative, i.e., $k_x < 0$ for planetary Rossby waves.

Notice that as was the case for inertia-gravity waves, the dispersion relation depends upon the stratification through R_d and Earth's rotation through f; notably, this dispersion relation also depends upon β.

The dispersion relation (12) is a very useful characterization of the linear, quasi-geostrophic vorticity balance Eqn. (10) and will be discussed here at some length. However, it is worth noting that plane Rossby waves — the literal interpretation of (11) — are generally *not* a prominent phenomena of the oceans. For example, there are no plane (long-crested) Rossby waves evident in Fig. 1, though in other years and other oceans, there may be, Sec. 2.6.2). Long-crested Rossby waves are not readily generated by winds and other forcing mechanisms, which generally have shorter space scales, and, even when they are, long-crested waves are likely to be unstable and evolve spontaneously into mesoscale eddies (an example is in Sec. 2.5). The perspective on Rossby waves taken here is that while Rossby waves are important in their own right, they are most important as the archetype of low frequency, nearly geostrophic motions generally, and including mesoscale eddies. The dispersion relation (12) is our handy guide to the relationship of time and space scales of such motions.

gyre. The term 'wave' might be applied reasonably to any phenomenon that results in the transmission of energy through a fluid (or solid) medium, though without necessarily transporting material. Mesoscale eddies on a beta-plane likely have just this property (Sec. 2.5) and so would qualify as waves in this (quite sensible) generalized sense. Here, however, the word 'wave' will be reserved here for an elementary plane motion of the sort Eqn. (11). Why this specific distinction between waves and eddies should be made clear in Sec. 2.7. (For a broad perspective on this issue see Scales, J. A. and R Sneider, 'What is a wave?', *Nature*, 401, 21 October, 1999, 739-740.)

Rossby waves are altogether different from the inertia-gravity waves of Part 2. In the first place, they have a very low frequency, and are very slowly moving; the factor in parentheses is O(1) for the wavenumbers and R_d of interest here and the frequency is determined largely by the leading factor, $\beta R_d \approx f R_d/R_E$ which is O(0.01)f, when $R_d = 40$ km, appropriate to the subtropical baroclinic ocean. This is the order of the frequency of both the numerical eddy and observed mesoscale eddies (Fig. 1). The frequency of Rossby waves is strongly dependent upon the wavenumber vector, i.e., both the magnitude and the direction. (This is in marked contrast to the isotropic dispersion relation of inertia-gravity waves on an f-plane noted in Part 2.) The east-west component k_x must be negative and so planetary Rossby waves propagate phase to the west only. For a given wavenumber magnitude, the frequency is a maximum when the wave vector is directed due west, $k_y = 0$, and the frequency is zero if the wave vector is directed due north or due south, $k_x = 0$. In that case the currents are purely east-west or zonal, and hence not subject to a β-effect. Zero frequency implies steady and exactly geostrophic motion, and any purely zonal motion satisfies Eqn. (12) regardless of k_y. The dispersion relation (Fig. 5) is symmetric north-south, and the north-south component of phase velocity can have either sign. The east-west component of phase speed is always negative, i.e., always westward (Fig. 6), a fundamental property of planetary Rossby waves.

The numerical (and the real) mesoscale eddies propagate almost due west, and hence it is helpful to simplify the dispersion relation to the case of an east-west wave vector, i.e., $(k_x, k_y) = (k_x, 0)$, Fig. (6),

$$\omega = -\beta R_d \left(\frac{R_d k_x}{1 + R_d^2 k_x^2} \right). \tag{13}$$

The phase speed in the east-west direction is

$$Cp \;=\; \frac{\omega}{k_x} = -\beta R_d^2 \left(\frac{1}{1 + R_d^2 k_x^2} \right) \tag{14}$$

and always negative (westward). The maximum phase speed occurs with the longest waves, and is up to βR_d^2, a stately 3 kilometers per day. The phase speed is, of course, a fundamental property of any wave, but nevertheless, the group speed is more evident in the experiments conducted here in which the waves spread from a confined region. The east-west group speed is

$$Cg \;=\; \frac{\partial \omega}{\partial k_x} \;=\; -\beta R_d^2 \left(\frac{1}{1 + R_d^2 k_x^2} \right) \left(1 - 2 \frac{R_d^2 k_x^2}{1 + R_d^2 k_x^2} \right), \tag{15}$$

which may be written

$$Cg \;=\; Cp \left(1 - 2 \frac{R_d^2 k_x^2}{1 + R_d^2 k_x^2} \right). \tag{16}$$

The group speed is westward for long waves, $R_d k_x \geq -1$, and also has a maximum magnitude of βR_d^2.

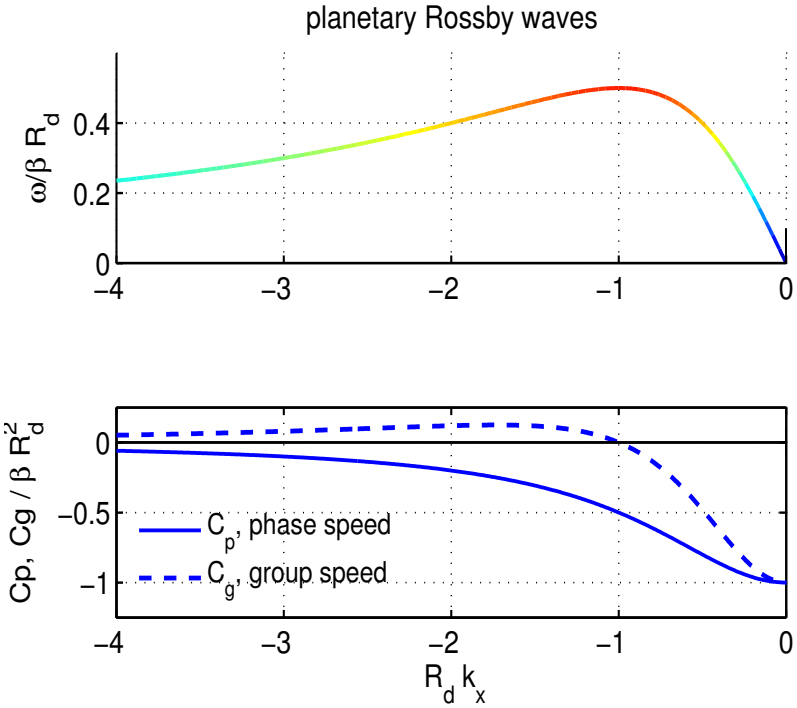

Figure 6: **(upper)** The dispersion relation for midlatitude, baroclinic, oceanic Rossby waves (Fig. 5) sliced along $k_y = 0$. Frequency is normalized by βR_d as before. **(lower)** Zonal phase and group speeds of planetary Rossby waves normalized by $\beta R_d^2 = 0.036$ m sec^{-1}. The phase speed (solid line) is always negative, i.e., always westward. The group speed (dashed line) is also westward for long waves, $R_d k_x \geq -1$, and is eastward and small for medium to short waves, $R_d k_x \leq -1$.

The phase and the group speed are proportional to β and so increase toward the equator. The group speed is eastward but rather slow even by Rossby wave standards for medium and short waves, $k_x R_d < 1$. The maximum eastward group speed is about $0.15\beta R_d^2$, or only about 1/2 kilometer per day at mid-latitudes, and occurs at $R_d k_x = -\sqrt{3}$. There is clear evidence of this slow eastward energy propagation in the idealized experiments that follow, but admittedly it is hard to see evidence of it in the real ocean.

In the preliminary discussion of the q-balance of Fig. (4), lower, it was noted that the β term is nearly balanced by the in-phase sum of relative vorticity and stretching vorticity. The next issue is the ratio of these two terms and the correlation of the ratio with the horizontal scale of the motion and the east-west distance from the starting point. This may be estimated from Eqn. (10) using that ∇^2 operating on a plane wave $\propto cos(k_x x - \omega t)$ gives $-k_x^2$ and thus,

$$\frac{relative}{stretching} = \frac{\frac{g'H}{f^2}\frac{\partial \nabla^2 \eta}{\partial t}}{\frac{-\partial \eta}{\partial t}} = \frac{g'H}{f^2}k_x^2 = R_d^2 k_x^2. \tag{17}$$

Relative vorticity is thus more important for waves which have a short horizontal scale, i.e. $R_d k_x \gg 1$, while stretching vorticity dominates for longer waves, $R_d k_x \ll 1$. The eddy of our geostrophic adjustment experiment has an initial scale $R_d k_x \approx 1$, so that relative and stretching vorticity terms are comparable in the initial q balance. By 365 days, the eddy has dispersed, especially east to west, and the q-balance has

become sorted out so that the ratio Eqn. (17) is about 4 in the vicinity of the eddy peak near $x = -1000$ km, and the ratio is about 1/4 in the region around x = 300 km. The east-west scale of the motion also varies systematically, being considerably larger toward the west than in the east. This east-west variation of the q-balance and of the horizontal scale of the motion are consistent with the Rossby wave dispersion relation.

2.3.1 Beta and relative vorticity; short Rossby waves

The presence of a wave implies a restoring force that is related to the configuration of the system. In the common case of simple harmonic waves in a fluid or solid, the restoring force is proportional to the displacement of a parcel away from equilibrium. The restoring force of a gravity wave is straightforward — gravity acting upon a displaced sea surface or internal density interface. The restoring 'force' of a Rossby wave must be related to the presence of β and the north-south displacement of parcels in a y-varying f. The restoring force provided by the β-effect is somewhat indirect compared to gravity acting on a displaced density surface, but nevertheless results in two quite different mechanisms of westward propagation and two kinds of Rossby waves, short Rossby waves and long Rossby waves. To follow along with the discussion below it will be helpful for you to make sketches of $\eta(x,t) = \eta_o cos(k_x x - \omega t), v(x,t)$, etc., and fill in the very brief calculations outlined here.

Suppose that the motion (waves) is in the short wave limit $R_d k_x \gg 1$. If $R_d k_x = 5$, say, then for $R_d = 40$ km, $\lambda \approx 50$ km would suffice. In that case, the relative vorticity term is considerably greater than the stretching vorticity term and the conservation of q may be approximated by the conservation of absolute vorticity

$$\xi + f = constant,$$

or in time-differentiated, linear form,

$$\frac{\partial \xi}{\partial t} + \beta v = 0, \tag{18}$$

a balance between *relative* vorticity and *beta*. A northward meridional current, $v > 0$, thus induces a negative change in the relative vorticity, $\frac{\partial \xi}{\partial t} < 0$, and the converse for a southward meridional current.

To see the westward phase propagation that results from this $q-$mode, assume that the meridional velocity has the form of a propagating plane wave,

$$v(x,y,t) = V cos(k_x x - \omega t),$$

with wavenumber directed due east-west. The zonal current then vanishes, and the relative vorticity is due solely to the east-west horizontal shear of the meridional velocity, $\xi = \partial v / \partial x$ (not the solid body

rotation that is often depicted in qualitative diagrams, e.g., the spinning cylinder in Part 2, Fig. (4), middle). Substitution of this plane wave form into the reduced $q-$conservation equation (18) then yields

$$\boxed{\omega = -\frac{\beta}{k_x}} \tag{19}$$

which is the short wavelength limit of Eqn. (14). The phase speed of short Rossby waves is then

$$\boxed{Cp_{shortRo} = -\frac{\beta}{k_x^2}} \tag{20}$$

and westward. $Cp_{shortRo}$ is obviously dependent upon k_x so that short Rossby waves are highly dispersive. Their group speed is

$$\boxed{Cg_{shortRo} = \frac{\beta}{k_x^2}} \tag{21}$$

and eastward, and notice equal in magnitude to the phase speed (Fig. 6).

The dispersion relation (19) is remarkable for what it omits: the dispersion relation (dynamics) of short Rossby waves does not depend upon the stratification or even the water column thickness; it depends only upon β and the zonal wavenumber, k_x. The motion is purely horizontal and nondivergent and so short Rossby waves are sometimes referred to as nondivergent Rossby waves. This is the $q-$conservation mechanism and the dispersion relation that C. G. Rossby inferred for westerly waves in the atmosphere (Secs. 1 and 2.6.1).

The group speed of short Rossby waves is very small, hundreds of meters per day as noted before, so that it takes quite some time for these waves to emerge from the initial eddy. But by day 365 there is clear evidence of slow, eastward energy propagation in the region $x > 200$ km (Fig. 4, lower). The horizontal scale in that easternmost region is, by inspection, $\lambda \approx 150$ km, and thus $R_d k_x \approx -2$, which is near the maximum eastward Cg. The linear q balance in that region is characterized by $relative/stretching \approx 4$. The very slow eastward extension of the eddy disturbance into the region east of the initial eddy position thus appears to be consistent with the slow eastward group speed and q balance of short(ish) Rossby waves.

2.3.2 Beta and vortex stretching; long Rossby waves

Another and very important mode of q-conservation holds for motions having a large horizontal scale in the sense that $R_d k_x \ll 1$. For the present case, $\lambda \geq 500$ km suffices. The change of relative vorticity is

negligible for such large scale motions, and the q balance may be approximated as (Fig. 4, lower, Part 2)

$$\frac{f}{H+\eta} = constant. \tag{22}$$

The linearized time rate of change is a balance between *beta* and vortex *stretching*,

$$\beta v \; - \; \frac{f}{H}\frac{\partial \eta}{\partial t} \; = \; 0. \tag{23}$$

To see how this q-mode may support a wave, presume a zonally propagating thickness anomaly

$$\eta(x,y,t) = \eta_0 cos(k_x x - \omega t)$$

that is in geostrophic balance with a north-south (meridional) current,

$$v(x,y,t) = \frac{g'}{f(y)}\frac{\partial \eta}{\partial x}.$$

Substitution into the reduced q-conservation equation and rearrangement yields

$$\frac{\partial \eta}{\partial t} = \frac{g'H\beta}{f^2}\frac{\partial \eta}{\partial x},$$

a first order wave equation. Substitution of the presumed plane wave form yields the dispersion relation

$$\boxed{\omega = -\beta\frac{g'H}{f^2}k_x} \tag{24}$$

the small $R_d k_x$ limit (i.e., the long Rossby wave limit) of Eqn. (14). The phase speed and the group speed are the same,

$$\boxed{Cp_{longRo} \; = \; Cg_{longRo} \; = \; -\beta R_d^2} \tag{25}$$

and independent of k_x. Long Rossby waves are thus nondispersive.

The dispersion relation of long Rossby waves depends upon stratification. Because the q-conservation mechanism of long Rossby waves is the β-induced divergence of the north-south (or meridional) geostrophic current, long Rossby waves are sometimes called divergent Rossby waves. Unlike the short Rossby wave, they can have a significant effect upon layer thickness, as we will see in Sec. 4. Notice especially the crucial f^{-2} dependence of the long Rossby wave phase and group speed. This will appear as a key, qualitative property at several junctures in this essay. An approximate $q-$balance of this sort is evident in the vicinity of the eddy peak, $-1200 \leq x \leq -800$ km, where the stretching term is about four times the magnitude of the relative vorticity term (Fig. 4, lower). The

wavelength is about $\lambda \approx 800$ km, and hence $R_d k_x \approx 0.3$, which is consistent with the ratio relative/stretching. The eddy peak at 365 days thus has a horizontal scale that is near the non-dispersive range of the Rossby wave dispersion relation (Fig. 6) and consistent with this, the eddy peak continues propagating westward with little further change and at a rate, 80 to 90% of βR_d^2, the long (Rossby) wave speed.

Though the eddy peak certainly does not have the appearance of a plane wave, it nevertheless has the q-balance and propagation characteristics of a (fairly) long elementary Rossby wave. Moreover, the propagation speed of the numerical eddy is consistent with the observed speed of oceanic mesoscale eddies at latitude 30^o. Most importantly, the satellite altimetry observations of Fig. (1) allow this result to be extended over a significant range of latitude.[6,7]

2.4 Finite amplitude effects, and the dual identity of mesoscale eddies

To now our discussion of eddy phenomena has emphasized that linear Rossby wave theory gives a very useful account of the westward propagation and dispersion seen in the η and $\mathbf{V}$ fields. This section will take a more in-depth look at the experiments and reveals two ways in which a linear description is incomplete: 1) First of all, there are modest but detectable finite amplitude effects on wave propagation in the base case experiment which has a realistic amplitude. 2) More striking is that fluid (tracer) transport by these eddies can be qualitatively different from the wave-like motion of the eddy peak and is entirely a finite amplitude effect. In this respect, mesoscale eddies have a kind of dual identity — Rossby wave-like when viewed in the η field, and yet capable of transporting tracer for significant distances depending upon amplitude. To highlight these phenomena and their dependence upon amplitude, it is helpful to compare the solutions from two new experiments made by setting the initial amplitude very small, $\eta_o = 1$ m (Fig. 7), so that all finite amplitude effects should vanish, and then much larger, $\eta_o = 100$ m (Fig. 8),

[6] A recent, comprehensive modelling study of the SSH climatology is by Early, J. J., R. M. Samelson and D. B. Chelton, 2011, 'The evolution and propagation of quasigeostrophic ocean eddies', *J. Phys. Oceanogr.,* doi: 10.1175/2011JPO4601.1 and references therein. Also highly recommended is http://jeffreyearly.com/science/qg-eddies-paper/ A notable, early theoretical/numerical study is by McWilliams, J. C. and G. R. Flierl, 1979, 'On the evolution of isolated, nonlinear vortices', *J. Phys. Oceanogr.*, 9, 1155-1182. A collection of research reviews is by Hect, M. W. and Hasumi, H., 2008, 'Ocean modelling in an eddying regime', *Geophys. Mono. Ser.*, **177**, American Geophys. Union.

[7] The discussion here was organized around two of the three modes of the linear potential vorticity balance that correspond with limits of the Rossby wave dispersion relation. Just to be complete, the third mode of vorticity balance is between stretching and relative vorticity, as in Fig. (4), upper, Part 2. In this mode, a change in relative vorticity occurs in phase with stretching, and thus when stretching stops, so does the change of relative vorticity. There is no mechanism for wave propagation associated with this mode, but it makes an important appearance in several numerical experiments; the geostrophic jets of Sec. 4.4, Part 2 exhibit this mode of q conservation, and there will be another example in Sec. 3.3 associated with Kelvin waves.

so that finite amplitude effects should be fairly pronounced.[8]

2.4.1 Eddy propagation seen in the η and V fields

The overall appearance of the normalized interface displacement $\eta(x,y,t)/\eta_o$ and the normalized current $\mathbf{V}/(C\eta_o/H)$ are not greatly different between these two experiments, but there are differences in detail. Most notably, the amplitude of the eddy peak is preserved somewhat longer in the large amplitude experiment and the waves found to the east of the peak have less symmetry when compared to the small amplitude experiment.

The zonal propagation speed of the eddy peak is also altered by finite amplitude effects: the zonal eddy peak speed is about 80% of $C_{longRo} = -\beta R_d^2$ in the small amplitude experiment (Fig. 9, dashed lines, and Fig. 10) and is about 90% of C_{longRo} in a large amplitude experiment, $\eta_o/H = 0.2$. For still larger amplitudes there is little further increase and so it appears that the long Rossby wave speed is a speed limit for the zonal motion of these eddies.

Finite amplitude effects cause a noticeable meridional motion of the eddy peak. Large amplitude anti-cyclones ($\eta_o/H = 0.1$, solid red line of Fig. 9) show a small component of motion toward the equator, about 10% of the westward propagation speed. Large amplitude cyclonic eddies show a similar poleward motion (the solid blue line of Fig. 9). These modest but detectable finite amplitude effects on the speed and direction of the eddy propagation seen in η are consistent with the observed propagation of oceanic mesoscale eddies seen in SSH (Fig. 1).[6]

2.4.2 Fluid transport seen in tracer fields and float trajectories

There is another very important class of eddy phenomena, the long term transport of fluid, often called the Lagrangian velocity, Part 2 Sec. 2, that is strongly dependent upon eddy amplitude. To see the fluid motion we have to analyze a tracer field or compute the trajectories of floats (passive particles). It was noted in Part 2 that the ideal (no external forcing) shallow water model has a natural, built-in tracer, the field of potential vorticity, q, which follows a conservation law, $Dq/Dt = 0$, i.e., q is conserved on fluid parcels. The initial condition on q (Fig. 11, left) in these experiments is a uniformly sloping background due to the northward increase of f, and a circular, low-q anomaly centered on $(x,\ y) = (0,\ 0)$ that is the

[8] This takes a short-cut. By the present definition of finite amplitude (Part 2, Sec. 2.3.4) we should first verify that there is indeed a linear regime at small amplitude by comparing the solutions from two (putatively) small amplitude experiments, say $\eta_o = 1$ m with $\eta_o = 2$ m, to verify that the scaled ηs and $\mathbf{V}$s are indistinguishable. They are.

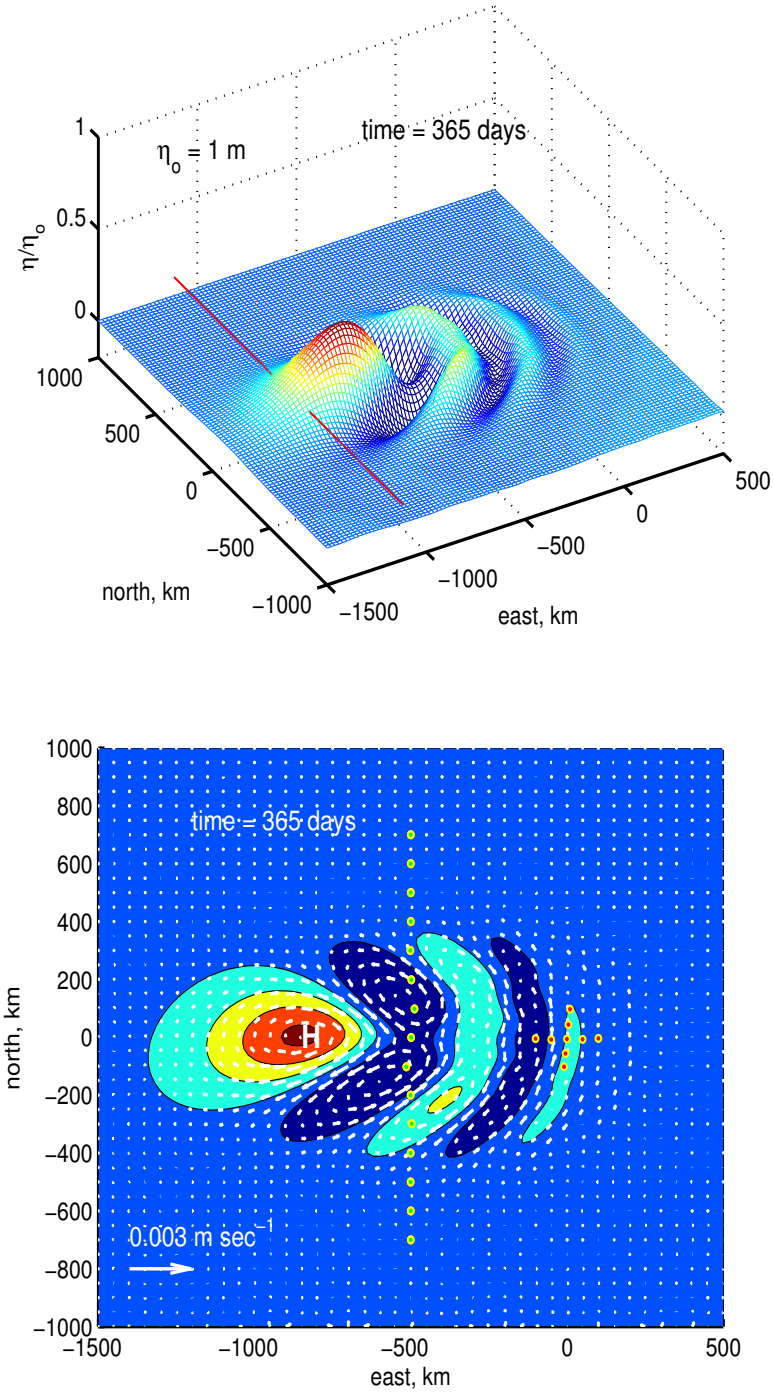

Figure 7: A small amplitude experiment in which $\eta_0 = 1$ m and $\eta_0/H = 0.002$ so that finite amplitude effects are negligible (a large amplitude experiment is next). **(upper)** The normalized interface displacement $\eta(x,y,t)/\eta_0$. **(lower)** The velocity field (vectors), thickness (color contours) and floats (red and green dots). The big vector at lower left has a magnitude $0.5C\eta_0/H$ and serves as scale for the velocity. The red floats were started within the eddy, while the green floats were set on a north-south line at $x = -500$ km and well to the west of the initial eddy. None of the floats moved an appreciable distance during the course of this year-long experiment, while the eddy peak propagated westward as if a linear wave. An animation of these data is pos1-u.mp4 in P3-videos.

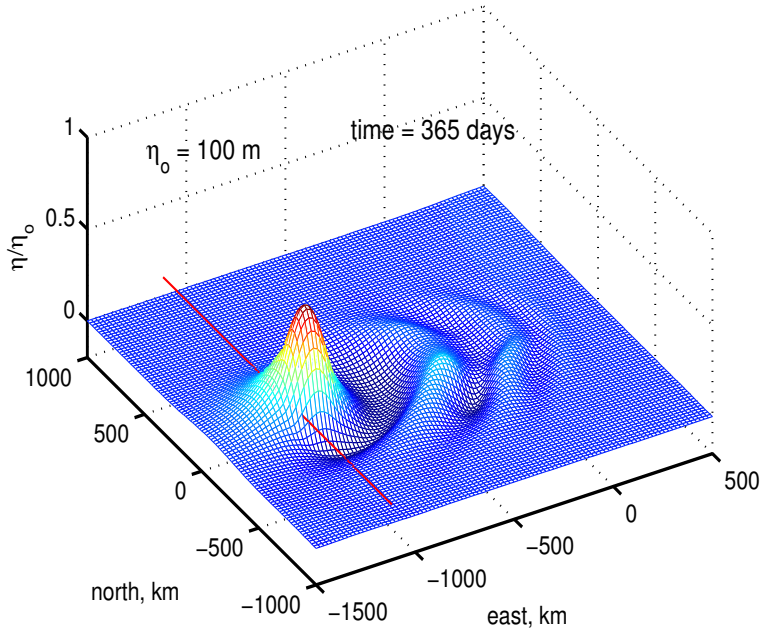

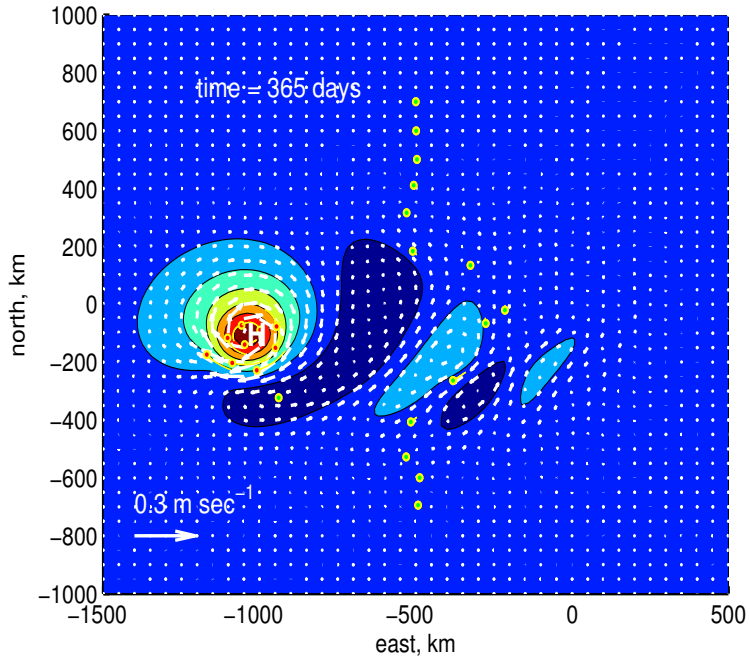

Figure 8: A large amplitude experiment, $\eta_0 = 100$ m and $\eta_0/H = 0.2$ so that finite amplitude effects are appreciable. **(upper)** Compared with the previous, small-amplitude experiment, Fig. (7), the (normalized) $\eta(x,y,t)$ eddy peak retained a somewhat larger fraction of its initial value. **(lower)** The velocity field and the floats of the large amplitude experiment. As before, the big vector at lower left has a magnitude $0.5C\eta_0/H$ and serves as the scale for velocity. The red floats, which were started within the eddy, were trapped by the eddy for the year-long duration of this experiment. The green floats, which were started well outside of the eddy along a north-south line at $x = -500$ km, were displaced mainly to the east as the eddy propagated by their initial longitude. The qualitative difference in these float trajectories compared to those of Fig. (7) shows that tracer (float) transport is a finite amplitude phenomenon. The animations provide a much more vivid sense of the differences between this and the previous experiment; this one is pos100-u.mp4

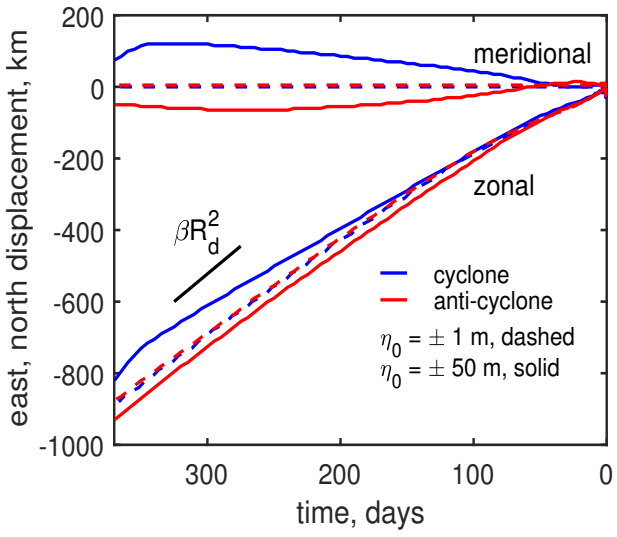

Figure 9: Time series of northward (here, poleward) and eastward displacement of the eddy peak (the maximum of $\mid \eta \mid$) for four experiments in which the amplitude and the sign of the initial displacement was $\eta_0 = \pm$ 1 m (two dashed lines that are almost identical) or $\pm$50 m (the solid red and blue lines). Blue curves are from the cyclones and red curves are from anti-cyclones. In all cases the zonal displacement is dominantly westward and at about 80 to 90% of the long Rossby wave speed, βR_d^2, evaluated at 30^{o}N. The strong cyclone (solid blue line) shows a small meridional poleward displacement (upper set of curves), while the strong anti-cyclone (solid red line) shows a small meridional equatorward displacement.

initial (thick) eddy. It is interesting to solve in parallel for the evolution of a passive tracer, $Ds/Dt = 0$, whose initial condition can be set arbitrarily; one simple choice is $s_o = 1$ inside the radius of the initial eddy, and zero otherwise (Fig. 12, left). The motion of the eddy center is readily apparent in the evolution of either of these tracer fields and is exactly the same in these two fields, as it should be. In the base case experiment, which has a fairly large amplitude, $\eta_o/H = 0.1$, the q or s anomaly moves mainly westward and slightly southward, very much like the eddy peak in this experiment. It bears emphasis that the tracer and the eddy q anomaly can move only by virtue of the fluid motion (not wave motion). Thus the appearance of the eddy's low q anomaly is associated with a noticeable contribution by the *nonlin* term to q conservation (Fig. 4, lower). The main contribution to *nonlin* is from horizontal advection of relative vorticity (the first term on the right side of Eqn. (8)).

The background (non-eddy) parts of these two tracer fields are somewhat different. The q field at the latitude of the eddy shows rather large meridional displacements of constant q lines. The passive tracer shows something similar only where there happens to be a meridional tracer gradient, near the eddy center and in a long, thin filament of tracer that extends from the eddy center back toward the starting location. This loss of tracer from the eddy into the filament is accompanied by a slow decrease of the eddy radius, mainly. The same filament is present also in the q field, although not apparent against the background of Fig. (11).[9]

[9]This tracer filament is very interesting insofar as it may show how discrete eddies may act to disperse tracer properties. However, this filament is also just the kind of thing that is especially challenging for a numerical solution. Specifically, the width of the numerical filament (i.e., the filament within a numerical solution) can never be less than several times the horizontal

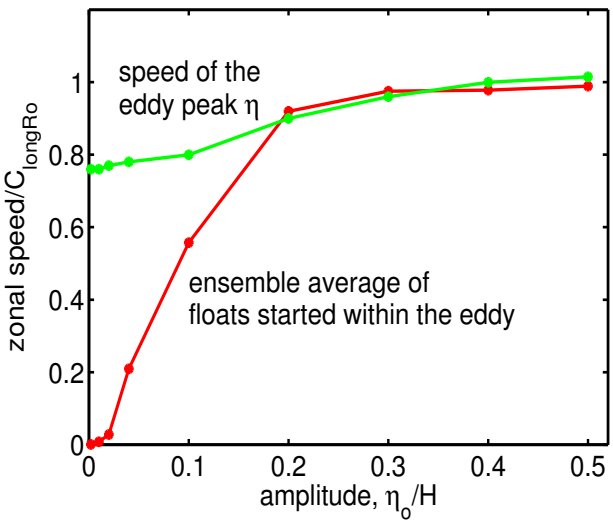

Figure 10: Average zonal speed of the eddy peak of η (green line; all anticyclones) and of an ensemble of floats that were launched within the eddy (red line) for nine experiments having amplitude $0.001 < \eta_o/H < 0.5$, the independent variable. The average is over the first year of the experiment. Speeds are normalized by the long Rossby wave speed at the average latitude of the eddy peak. The normalized eddy peak speed depends somewhat upon the eddy amplitude, while the ensemble-averaged float speed is very sensitive to eddy amplitude up to $\eta_o/H \approx 0.2$. These are robust results in a numerical solution sense, and an interesting comparison of two important properties of (numerical) mesoscale eddies. However, the eddy peak speed and the ensemble-averaged float speed (or Lagrangian velocity) are, in general, qualitatively different things, e.g., the float speed depends upon the averaging interval in the intermediate amplitude cases in which some fraction of the floats is lost from the eddy during the first year (as in Fig. 4, upper).

Fluid motion may be easier to quantify when diagnosed from the motion of discrete, passive parcels, or 'floats' (Sec. 2.3.3, Part 2), that are set in the initial state. A cluster of nine (red) floats was started within the eddy to serve as a tag on the eddy, and a line of (green) floats was placed along a north-south line 500 km west of the eddy initial position (Fig. 7, lower) to show the motion of the ambient fluid as the eddy passes through their longitude. In the small amplitude experiment, $\eta_0/H = 0.002$ (Fig. 7), all of these floats appear to be essentially frozen in space for the full duration of the experiment. At the same time, the eddy marked by η moves westward as would a linear Rossby wave. The ensemble average speed of the red floats launched within the eddy is thus about zero, while the eddy peak defined by η propagates at about 80% of C_{longRo}. This qualitative difference between float (and thus fluid) motion and

grid interval, 5 km, which may be considerably greater then the natural, physical horizontal scale of the filament. Small changes in the diffusion (deliberate or numerical) or even in the method used to estimate and time-step the advection terms of the tracer equation can thus cause a significant difference in the width of the filament and thus in the tracer concentration along the filament, even while leaving the eddy propagation almost unaffected. Eddy propagation thus appears to be a robust and well-resolved process in these numerical solutions, while the width and tracer concentration along this very thin tracer filament are not.

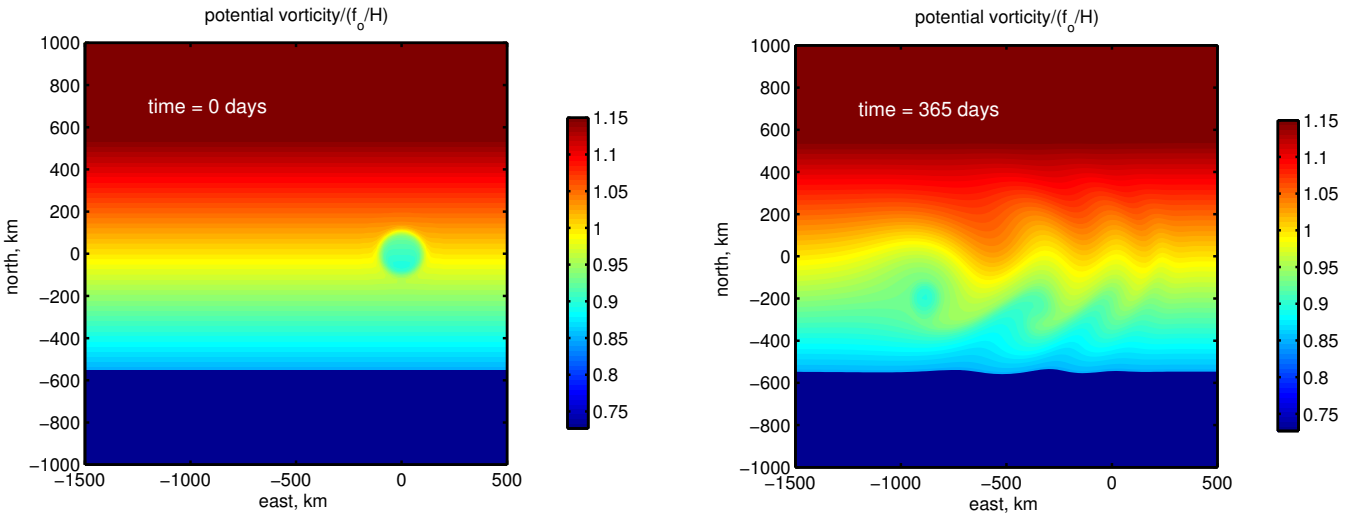

Figure 11: Potential vorticity from the experiment $\eta_o = 50$ m. **(left)** The initial condition. The eddy is the pale blue, low q anomaly centered on $(x,y) = (0,0)$. **(right)** At 365 days. The eddy center marked by the potential vorticity anomaly is now at $(x,y) = (-900,-200)$ km, which is about 100 km equatorward of the eddy peak seen in η at this time.

the motion of the eddy peak seen in η also leads to the depiction of the eddy peak motion as 'propagation', and implicitly, wave propagation.

The float movement (and the transport of tracers and fluid) is very different in the large amplitude experiment, $\eta_o/H = 0.2$, (Fig. 8, lower), even while the westward propagation of the eddy peak is changed only slightly. The large amplitude azimuthal current within the eddy effectively traps the red floats on the side of the eddy where the current is westward, in the direction of the eddy propagation (the south side of the anticyclone of Fig. (8, lower). The eddy then advects the floats to the west-southwest over a distance of almost 1000 km within the first year. The long-term, ensemble mean Lagrangian velocity of these specific floats is thus the same as the speed of the eddy peak (Fig. 10), about 95% of C_{longRo}. In an intermediate amplitude experiment, roughly $0.03 \leq \eta_o/H \leq 0.2$, e.g., Fig. (4, upper), some fraction of the red floats are lost from the eddy as it shrinks in radius during the first year, and hence the ensemble-average float speed is intermediate between 0 and the eddy peak speed. The ensemble-average float speed thus depends entirely upon the residence time of the floats within the eddy, which in turn depends upon the initial amplitude of the eddy and the rate at which it decays and disperses. This significant dependence of the float speed with amplitude fits the present definition of a finite amplitude phenomenon.[10]

[10]The meridional drift of large amplitude eddies has been studied extensively in the context of tropical cyclone motion, see http://www.aoml.noaa.gov/general/WWW000/nhurr00.html . In brief, the present eddies have a horizontal scale $KR_d \leq 1$ that

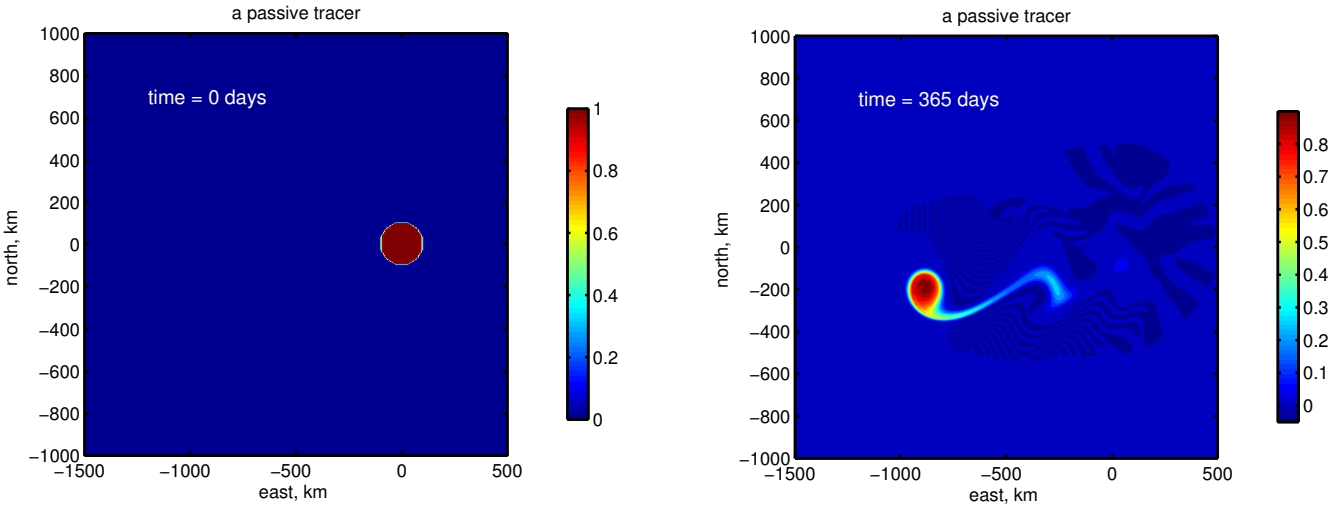

Figure 12: The evolution of a passive tracer inserted into the experiment $\eta_o = 50$ m. **(left)** The initial condition; $s = 1$ within the initial eddy, $s = 0$ otherwise. **(right)** At 365 days. Notice that the eddy center marked by tracer is at about $(x, y) = (-900, -200)$ km, and the same as seen in the q field of the previous figure. Notice too the thin, wispy trail of tracer left behind the westward-propagating eddy. This corresponds with the line of (red) floats dropped off by the eddy Fig. (4, upper) and with a faint local minimum of potential vorticity.

2.5 Rossby waves → Eddies

This essay has discussed Rossby waves (elementary, plane Rossby waves) and mesoscale eddies on a more or less equal footing. This may have left you wondering if these phenomenon are equally important and whether there may be connections between them, even aside from their common vorticity balance. One interesting connection is that under common circumstances, Rossby waves are expected to evolve spontaneously into mesoscale eddies, i.e., Rossby waves are very often unstable. The topic of fluid flow instabilities is beyond the scope of this essay, but a simple example of Rossby wave instability will serve to illustrate the phenomenon and (ideally) may stoke your appetite for more.[11]

---

is not completely large scale, i.e., the beta effect is not balanced solely by divergence. There is some relative vorticity generated by the meridional velocity of the eddy and an induced cyclonic vorticity on the northeast side of the eddy and cyclonic vorticity on the southwest side. The net result is a markedly asymmetric velocity field with a strong southwest current on the southern side of the eddy, readily evident in Fig. 8, bottom. This current acts to self-advect the eddy center toward the southwest. For a large amplitude cyclone the strongest current is on the northeast quadrant and is directed northwest. The amplitude of this current is much, much greater than the resulting southwest drift of an anti-cyclonic eddy (noted in the discussion above), evidently because it is on the periphery of the eddy, and is directed mainly along lines of constant h.

[11] See Isachsen, P. E., J. H LaCasce and J. Pedlosky, 'Rossby wave instability and apparent phase speeds in large ocean basins', *J. Phys. Oceanogr.*, 2007, 1177-1191, DOI: 10.1175/JPO3054.1 and references therein.

The model is initialized with a rather special state: a north-south oriented ridge/trough that mimics one isolated wave,

$$\eta(x,y,t=0) \;=\; \eta_o \frac{f}{f_o} \sin(2\pi x/\lambda) \quad \text{if} \quad |\,x\,| < \lambda/2, \tag{26}$$

and otherwise

$$\eta(x,y,t=0) \;=\; 0 \quad \text{if} \quad |\,x\,| > \lambda/2.$$

The wavelength is $\lambda = 600$ km. The currents are initialized with the corresponding geostrophic velocity. The evolution of this system is dependent upon amplitude, and so it is desirable to make the initial current the same at all latitudes. The amplitude was therefore scaled with f/f_o, with f_o appropriate to 30^oN. In the first experiment the amplitude is very small, $\eta_o = 1$ m and thus $\eta_o/H = 0.002$; in a second experiment the amplitude is very large, $\eta_o 100$ m and thus $\eta_o/H = 0.2$. In an attempt to minimize the effect of northern and southern boundaries of the model domain, the amplitude was tapered to zero approaching the equator and also at very high latitude (off of the model domain shown here).

Once this feature is released onto a β-plane we would expect westward propagation as a (fairly) long Rossby wave, and indeed that happens. There is quite noticeable dispersion since the isolated sinusoid Eqn. (26) is not a pure harmonic. As well, while the initial wavelength is long, $kR_d \approx 0.4$, it is not extremely so. When the initial amplitude is very small, $\eta_o/H \ll 1$, (middle panel of Fig. 13), the wave remains easily identifiable for O(1000) days and the leading edge just about keeps pace with the expected long Rossby wave speed. When the amplitude is very large, $\eta_o/H = 0.2$ (lower panel of Fig. 13), the evolution is dramatically different. Within a few hundred days there appears a semi-regular train of lumps and bumps along the length of the wave, and by about 500 days the original long-crested wave evolves into a semi-regular array of mesoscale eddies. These eddies have a scale (diameter) of about 250 km in the northern (high latitude) portion of the domain, and somewhat larger, about 400 km in the low latitude part of the domain. These eddies are in the small wavenumber region of kR_d space, and so they too propagate westward at a rate that is just slightly less than the initial Rossby wave propagation. Even though the initially smooth and continuous wave breaks up rather dramatically, westward propagation nevertheless continues almost unabated.

The details of when and where the eddies form in this experiment depends sensitively upon the way that the initial wave is perturbed. Here the perturbation results mainly from the low latitude end of the wave, which recall was tapered to fit into the model domain. The real ocean is filled with all manner of perturbations having a wide range of time and space scales, though probably nothing quite like the tapering employed here. In any event, the result of the instability — mesoscale eddies — is not sensitive to the form of the perturbation.

Theory (see Isachsen et al.[11]) indicates that the scale of the most rapidly growing instability is proportional to the local radius of deformation, consistent with the y-dependent diameter of the mature

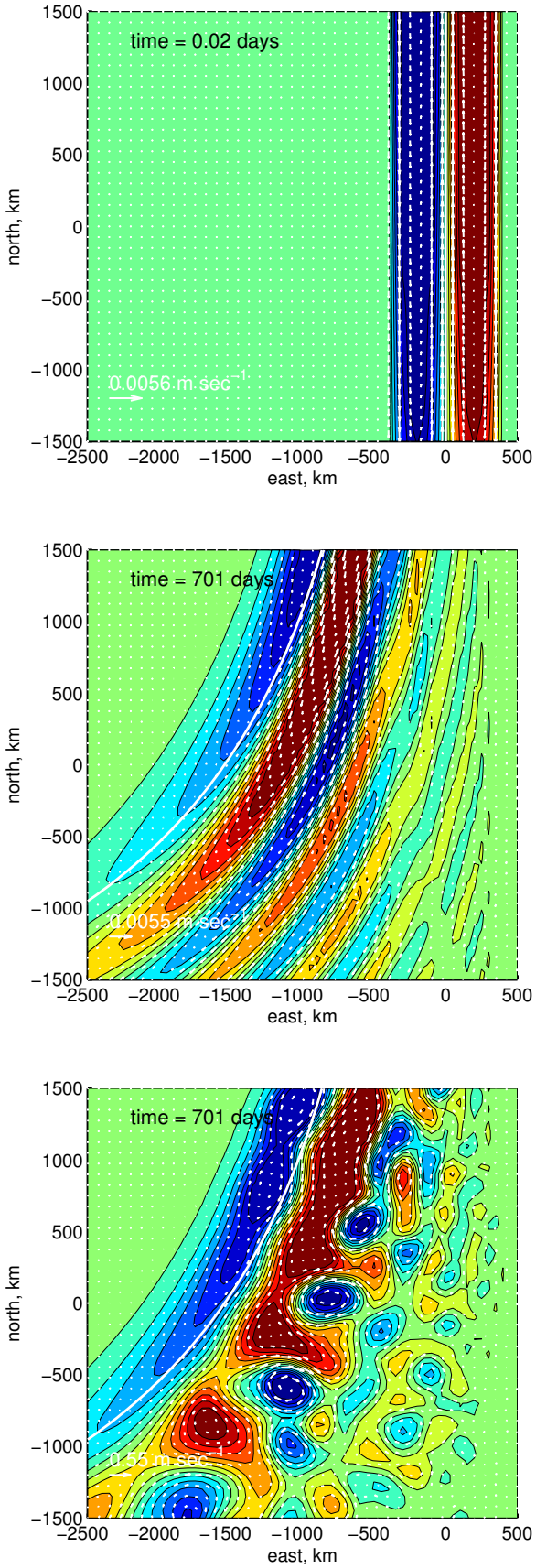

Figure 13: Two experiments that were initialized with a single meridionally-oriented wave in geostrophic balance. **(upper)** The initial condition. **(middle)** The normalized thickness anomaly and currents of a small amplitude case that had η_o = 1 m. The white parabola was started at $x = 0$ and then displaced westward at the y-dependent long Rossby wave speed. The leading ridge/trough just about keep pace with this westward speed but there is also significant dispersion, with shorter wavelengths lagging well behind. **(lower)** A large amplitude experiment having η_o = 100 m.

eddies found here. The rate at which the instability grows (once triggered by some kind of perturbation) is expected to be proportional to the amplitude of the initial wave. The two cases of Fig. (13) are extreme, $\eta_o = 1$ m and $\eta_o = 100$ m. In the former case the growth is so slow that there is little evidence of eddy formation even after almost two years. However, in the large amplitude case, which is closer to being realistic of the ocean, the growth is fairly fast, with eddies becoming apparent within several hundred days of the start of the experiment.

2.6 Appendix: Some of the varieties of Rossby wave-like phenomenon

2.6.1 Westerly waves

The westerly wind belts that encircle the mid-latitudes in both hemispheres are nearly always perturbed by wave-like undulations, appropriately termed westerly waves, that are a very significant factor in the day-to-day variation of weather (Fig. 1, Part 1). The longest such waves having wavelengths of O(10,000 km) are often observed to be almost stationary with respect to Earth despite that they are embedded in the eastward flowing westerly wind belt where the spatially-averaged wind is $\bar{U} \approx 30$ m s^{-1}. The longest waves have a westward propagation speed that is just sufficient to stem this eastward advection and may appear to be nearly stationary with respect to the Earth. Quasi-stationary waves of this sort are very common in fluid flows around fixed obstacles: 'rapids' on the surface of a river and ripples on the flow of water from a faucet are familiar examples.

On the other hand, the shortest westerly waves, which may dominate the instantaneous pattern of the westerlies at other times (the web site noted in footnote 3, Part 1 shows instances of this) clearly propagate from west to east. In some cases short waves move eastward at a speed that is not much less than $\bar{U}$. Short westerly waves (which have wavelengths of several thousand kilometers) thus appear to be almost passively advected by the westerly wind. Rossby proposed that westerly waves propagate zonally within a zonal mean flow, $\bar{U}$, as

$$C_w = \bar{U} - \frac{\beta}{k_x^2}, \tag{27}$$

which is the short (non-divergent) limit of the Rossby wave dispersion relation Eqn. (12) plus advection. This relation, and the analysis that led to it, proved to have great merit both as a fundamental explanation of the observations and as a practical guide for weather forecasting.[12]

[12] A superb animation of westerly waves is at https://oceanservice.noaa.gov/facts/rossby-wave.html

2.6.2 Basin-scale Rossby waves

Satellite altimetry has revealed that most ocean basins are full of low frequency variability. In the lower subtropics, a portion of the low frequency variability takes the form of very long-crested, westward propagating, baroclinic features that are unambiguously planetary Rossby waves. These long-crested waves originate on or near the eastern boundary, and then may propagate a very long distance into the open ocean (Fig. 14). This phenomenon makes clear that something very close to an elementary Rossby waves can indeed occur in the ocean, provided that some mechanism has the appropriate (long) time and (long) space scales needed to generate them in the first place.

A remarkable occurrence of such a long-crested Rossby wave was observed in the Pacific ocean in the decade following the very large amplitude ENSO event of 1982-1983.[13] The ENSO event began with a slackening of easterly winds over the western tropical Pacific ocean that allowed the very thick western tropical thermocline to relax back toward a lower energy state, something like the release of our raised eddy of Secs. 4.1 and 4.2, though on a much larger scale. The fastest response was a positive (relative high of SSH and a thick upper layer) Kelvin wave pulse that propagated from the western Pacific to the eastern boundary of the Pacific (roughly 15,000 km) within about two months; $C \approx 3$ m sec^{-1}. The equatorial Kelvin wave was scattered into positive boundary Kelvin waves that propagated north and south along the eastern boundary at a similar speed. The arrival of a positive Kelvin wave is accompanied by warm poleward currents and a thickened thermocline that have very significant consequences for coastal ecosystems (El Nino of the eastern South Pacific). The thickened thermocline along the eastern boundary was the proximal forcing mechanism of baroclinic Rossby wave(s) that began propagating westward across the Pacific basin. The meridional extent of the waves (distance along the wave crest) was more than 3000 km in both hemispheres, the meridional extent of the boundary Kelvin wave disturbance. Wave crests were strongly refracted toward the west at low latitudes (Fig. 14), consistent with the wave speed of long (divergent, non-dispersive) baroclinic Rossby waves, $C \propto \beta/f^2$, i.e., faster westward propagation at lower latitudes (but not in excess of C). The initial, high SSH wave pulse that started the 1982-1983 ENSO event was detectable for at least a decade after its generation, by which time it had reached the western boundary near Japan, where it altered the path of the Kuroshio current. This kind of very large scale, low frequency variability is predictable for years ahead, once it has formed.

One question these observations raise is, how could such a long-crested wave survive the instability process noted in Sec. 2.7? The satellite SSH observations that were made in the 1980s were not as well resolved spatially as those made more recently, but a second look at the field of (Fig. 14) suggests that the wave front may very well have fractured into mesoscale eddies. As we have seen, these eddies propagate to the west very much like the original, long-crested Rossby wave.

[13] Jacobs, G. A., H. E. Hurlburt, J. C. Kindle, E. J. Metzger, J. L. Mitchell, W. J. Teague, and A. J. Wallcraft, 1994: 'Decade-scale trans-Pacific propagation and warming effects of an El Nino anomaly', *Nature*, Vol. 370, pp. 360-363.

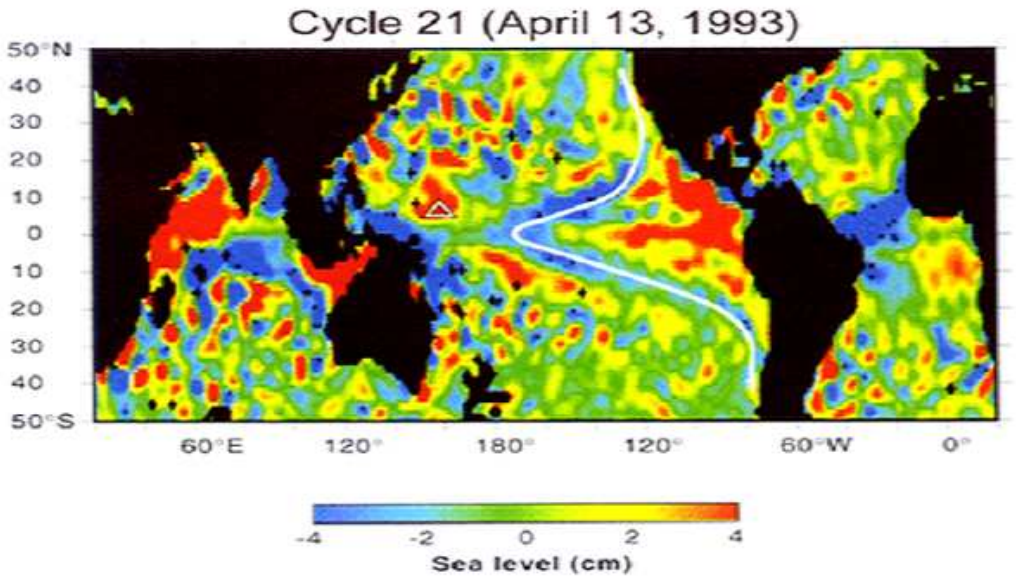

Figure 14: A snapshot of SSH observed by TOPEX/POSEIDON satellite altimetry in the Spring of 1993. The subtropics in both hemispheres of the Pacific basin showed long-crested, westward propagating baroclinic Rossby waves that started on the eastern boundary. The white line is along a relative low of SSH. The westward refraction of the wave crest at low latitudes is consistent with the latitudinal dependence of a long (divergent and non-dispersive) baroclinic Rossby wave. Notice that there is similar variability evident also in the Atlantic basin (though evidently not in 2007, Fig. 2). This figure is reproduced with permission from Dudley Chelton, and is from Chelton and Slax (1994), https://oregonstate.app.box.com/s/oetv6qnepc9go6ruhp4cnqab2e6gbi9d

2.6.3 Topographic eddies and waves

The variation of bottom depth has been omitted from our analysis, mainly for simplicity. This would be an acceptable approximation in cases where the flow of wind or ocean currents at the ground or sea floor was very weak, as in the mesoscale eddies of Sec. 2 or the open ocean, equatorial phenomenon of Sec. 3. However, there are common circumstances where strong currents occur near the bottom even in the deep, stratified ocean, e.g., under the Gulf Stream, and circumstances where the flow is barotropic (depth-independent) and hence in contact with the bottom, e.g., on continental shelves. The relevant, background potential vorticity is then $f/(H+b)$, with $H+b(x,y)$ the nominal thickness. The essential difference between column thickness that varies with b vs. η is that b is spatially dependent but time independent. A fluid column that moves across bottom contours will then necessarily be stretched (or squashed), inducing relative vorticity, exactly as does flow across lines of constant f.

The ratio of planetary to topographic vorticity change over a typical continental shelf is

$$\frac{\text{planetary}}{\text{topographic}} = \frac{\frac{1}{f}\frac{\partial f}{\partial y}}{\frac{1}{h}\frac{\partial h}{\partial y}} = \frac{h}{\alpha R_E} \text{ is } O(10^{-1}),$$

given a bottom slope $\alpha = 10^{-3}$ and nominal depth $H = 200$ m. The magnitude of the topographic term can easily exceed the planetary β term since the bottom depth typically varies on much shorter spatial scales than does f (radius of Earth, R_E). Topographic effects would prevail over the (planetary) β-effect over most of the deep, open ocean as well, except that stratification largely shields the upper water column from direct bottom slope effects. Assuming that topographic variation dominates the gradient of the background potential vorticity, $q = f/H$, and that the flow is depth-independent, then the frequency of topographic Rossby waves is given by

$$\frac{\omega}{f} = \frac{\alpha g}{fC}\left(\frac{R_d K}{1 + R_d^2 K^2}\right),$$

where $R_d = C/f$ is the barotropic radius of deformation, with $C = \sqrt{gH}$ computed from a nominal H and the full gravity. For a nominal shelf, $C \approx 45$ m s^{-1} and $R_d \approx 900$ km (mid latitudes). These waves often have considerably higher frequencies than do planetary Rossby waves, with 5 - 20 day periods being common. They have correspondingly greater phase and group speeds as well. Just as planetary Rossby waves propagate phase westward - with higher background potential vorticity to the right of the wave vector - so too these topographic Rossby waves propagate phase with shallower water and thus larger f/H on their right.[14]

2.6.4 Tropical cyclones

One of the most remarkable instances of Rossby wave dynamics occurs in conjunction with tropical cyclones (TC), intense vortical flows around low pressure anomalies. Most TCs begin with a convective cloud cluster, that may become organized into a vortex and grow in amplitude and scale if the mesoscale shear environment includes sufficient cyclonic vorticity. Mature TCs typically have a radius of several hundred kilometers, which is quite small compared to the atmospheric radius of deformation, about 1000 km.

Some tropical cyclones (about 1 in 6) have been observed to develop a marked, eastward-extending Rossby wave wake in the troposphere. The wavelength along the wake is typically several thousand

[14] An excellent description of short-crested, baroclinic, topographic waves (or eddies) observed under the Gulf Stream is available at http://www.po.gso.uri.edu/dynamics/wbc/TRW.html

kilometers, and consists of alternate cyclonic and anti-cyclonic disturbances. The cyclonic features have been observed to act as the vorticity trigger for subsequent TC genesis, so that TCs, particularly in the western North Pacific, may develop in a semi-regular sequence at intervals of several thousand kilometers. The spatial scale is evidently set by the Rossby wave properties of the eastward extending wake.[15]

2.7 Problems

(1) A little more on high frequency beta-effects. Imagine an f-plane, and an initial condition that is an unbalanced and unforced northward current in a surface layer of thickness h. How would the resulting free inertial motions evolve at two sites at different latitudes? Now suppose that this experiment is repeated but on a beta-plane and taking account of the possible pressure gradient that would follow from divergence of the upper layer current. How would the inertial oscillations evolve? Now suppose that the initial condition is consistent with generation by a wind with some duration so that $v \propto \tau/(f(y)h)$. If you followed this, then you can appreciate that there are two high frequency beta-effects; a y-dependent frequency of inertial motions, and a $1/f(y)$ dependence of wind-driven current amplitude.

(2) Eqn. (13) is the third time that the radius of deformation has arisen as the appropriate length scale against which to compare (or measure) horizontal scales, in that case the wavelength of Rossby waves. Does this reflect an excess of enthusiasm for R_d, or is there really nothing else as suitable? What about the layer thickness, H? Surely it too is an intrinsic length scale.

(3) Rossby waves exhibit normal dispersion in that longer waves have greater phase speed. It can happen that shorter waves have a greater phase speed, a property dubbed anomalous dispersion. An example of anomalous dispersion that you can readily investigate is that of capillary waves generated by the movement of a small object across the surface of still water. If the object moves more slowly than the slowest gravity/capillary wave, there are no waves. But when the speed of the moving object exceeds this minimum wave speed, a wave pattern will suddenly appear around and in front of the object. Short capillary waves lead the pack. Here's a question for you to answer experimentally: at what speed does this occur? (A factor of two is fine.) Anomalous and normal dispersion may be investigated also via numerical experiments that solve an initial value problem, ftransform.m (Sec. 7, Part 2).

(4) A couple of dispersion relation questions for you: 1) Sketch the dispersion relations for the short and long Rossby waves limits onto Fig. (6, upper). Use parameters appropriate to 30^o N; f = 7.29x10^{-5} sec^{-1}, $C = 3$ m sec^{-1}, and β = 1.98x10^{-11} sec^{-1} m^{-1}. 2) Discuss the phase and group speed in the case that $KR_d = 1$, and interpret Fig. (4, lower).

(5) Westward energy propagation is the dominant outcome of the β plane experiments and got most of our attention, but there is noticeable eastward energy propagation as well. Starting with Eqn. (13), show that the maximum eastward C_g is $C_{longRo}/8$ and occurs at $R_d k_x = \sqrt{3}$.

[15] This phenomenon is an active area of research, see Krouse, K. D. , A H. Sobel and L. M. Polavni, 2008, 'On the wavelength of the Rossby waves radiated by tropical cyclones', *J. Atmos. Res.*, 65, 644-654, and references therein.

(6) Evaluate the long Rossby wave speed over the latitude range 10 to 50^o. In this you may assume that the gravity wave speed C is constant, $C = 3$ m sec^{-1} (though in fact it decreases somewhat poleward of the subtropics). You will notice that the latitudinal dependence of the long Rossby wave speed is quite pronounced. Can you explain in a few words where this f^{-2} dependence originates?

(7) Some eddy propagation questions. 1) How does your result from the problem 4) above compare with the eddy propagation speed found in the numerical experiments? The experiment of Fig. (3) takes care of 30^o N, so you will need to find the numerical result for other latitudes. Much better that you design and run the experiments yourself, but in case that is not feasible, some animations for other latitudes are linked in Sec. 7, Part 2. We noted in the discussion of Fig. 1 that the observed propagation speed of oceanic mesoscale eddies varies significantly with latitude, being considerably faster towards lower latitude. On average over all ocean basins the observed[1] (latitude, zonal speeds) are (10^o, -14 ± 4 cm sec^{-1}), (20^o, -5.0 ± 1.5 cm sec^{-1}), (30^o, -3.5 $\pm$1.5 cm sec^{-1}), (40^o, -1.5 $\pm$1 cm sec^{-1}) and (50^o, -0.8 $\pm$ 0.5 cm sec^{-1}). How does this compare with your results above?

(8) The natural way to think of conservation is following a given parcel or water column, i.e., a Lagrangian description. Our model equations are, however, Eulerian. 1) Go back and make an explicitly Lagrangian description of the two q conservation modes discussed above (short and long Rossby waves), and then make the corresponding Eulerian description.

(9) The discussion in the main text emphasized the trajectories of the floats that were set inside the initial eddy (the red floats). What happens to the green floats that were launched outside and to the west of the eddy? Consider the small and large amplitude experiments, Figs. (7) and (8) and their animations.

3 Adjustment on an equatorial β-plane

The temporal and spatial variability of equatorial SSH is very different from that seen at subtropical and higher latitudes. Mesoscale eddies are uncommon (though appear seasonally in some years in the Pacific), and a gyre-like structure is not readily apparent.[16] The main features are:

1) The primary variability of SSH is in zonally elongated features. These have a meridional scale of several hundreds of kilometers, and widths that may span most of the Atlantic basin. These features exhibit strong seasonality.

2) SSH variability has small amplitude. Aside from the western boundary current, the amplitude of SSH variability is typically $\pm$ 0.05 m, compared with $\pm$ 0.1 to 0.2 m for mesoscale eddies of the

[16]Most of the equatorial phenomena described here are seen much better in multi-year records: a superb animation of 18 years of satellite-derived altimetric data including the Pacific and Indian oceans is available from http://podaac.jpl.nasa.gov/node/430

subtropics and ± 1 m over the subtropical and subpolar gyres. f is, of course, much smaller, and so this does not mean that currents are also small amplitude.

3) Episodic, eastward propagation over distances that may span most of the basin.[16] The propagation speed of these eastward-going events is comparable to the gravity wave speed, several hundred km per day.

3.1 An equatorial adjustment experiment

The plan for this section is to carry out a geostrophic adjustment experiment on an equatorial beta-plane ocean and compare the results to previous experiments. As before, the motive is to gain some insight into the properties and mechanisms of the observed SSH noted above. To be sure, the results of this adjustment experiment can account for only a part of these equatorial phenomena, much of which is due instead to forcing by the large-scale, time-dependent equatorial winds. Hence, some of the discussion is deferred to Part 4. Here in Part 3 we will emphasize the properties of equatorial waves, which are of first importance in understanding variability generally.[17]

The β-plane is set to $f_0 = 0$ and $f = \beta y$, i.e., an equatorial β-plane. The stratification was changed somewhat to reflect the shallower main thermocline of equatorial regions, H = 250 m, and larger density contrast across the main thermocline, $\delta\rho = 3$ kg m^{-3}. The gravity wave speed $C = \sqrt{g'H} \approx 2.5$ m sec^{-1}. The initial condition is a raised, cylindrical thickness anomaly with radius $L = 200$ km that is centered on the equator. Though this eddy is twice the size used previously, it is nevertheless small compared to the intrinsic horizontal scale of the equatorial ocean. The domain is a box 5000 km by 5000 km. The northern and southern sides are treated with a radiation boundary condition that allows the passage of gravity waves off of the model domain. The eastern and western sides are defined by zero normal flow, $u(x = \pm 2500) = 0$. Waves reaching the zonal boundaries are thus reflected and scattered.

Soon after the equatorial thickness anomaly is released, Fig. (15), gravity waves propagate away in all directions. The leading edge of the expanding wave front is nearly circular, and grows in radius at the gravity wave speed $C = \sqrt{g'H}$, as seen before. Within about a week, gravity wave motions dispersed (spread) the eddy energy over most of the model domain. The initial thickness anomaly collapsed within about $L/C \leq 1$ day, very much as would be expected in the complete absence of rotation (Sec. 3.1, Part 2). The initial condition was symmetric about the equator, and this north-south symmetry is maintained in all that follows. However, the waves showed some significant east-west anisotropy, with preferred

[17] The GFD text by Gill noted in footnote 1 of Part 2 has a very useful discussion on equatorial dynamics. One of the seminal research papers on equatorial dynamics is also highly recommended: Matsuno, T., 1966, 'Quasi-geostrophic motions in an equatorial area', *J. Met. Soc. Japan*, 44(1), 25-43.

propagation along the equator and especially eastward, as will be discussed further below. These very significant details aside, this equatorial adjustment process looks more like the pure gravity wave experiment of Sec. 3 Part 2 than the mid-latitude f- or β-plane experiments. Beta is almost the same in this experiment as in the mid-latitude experiments of Sec. 2, and so it isn't β alone that matters but mainly f_o (which is zero here).

3.2 An equatorial radius of deformation

In the $f-$plane and mid-latitude $\beta-$plane experiments of previous sections, the radius of deformation, $R_d = C/f_0$, was the intrinsic horizontal scale against which to measure the radius of the initial eddy, wavelengths, etc. On an equatorial $\beta-$plane, $f_0 = 0$, and so the equivalent radius of deformation, R_{deq}, is bound to be somewhat different. How might this R_{deq} be deduced? Three possibilities: 1) Look for the radius of deformation in a solution involving transcendental functions of the north-south coordinate. An example is coming in the next section, but very often an explicit solution will not be available, and then something more general will be required. 2) Apply the method of dimensional analysis to deduce a length scale from the parameters that define the ocean model. Dimensional analysis works particularly well in this instance because there are only two parameters that define a shallow water, equatorial β-plane, the gravity wave speed, C [length time^{-1}] and of course β [length^{-1} time^{-1}]. The simplest, dimensionally consistent form of a length is

$$R_{deq} \;=\; \sqrt{C/\beta}, \tag{28}$$

which turns out to be correct. This result came awfully easily, but without the slightest hint of a physical interpretation. 3) Finally, recall that the long Rossby wave speed increases toward lower latitude as $\beta R_d^2 = \beta C^2/f^2$ and on an equatorial beta-plane, $\beta C^2/(\beta y)^2$. This cannot hold hold all the way to the equator, $y = 0$, since the fastest possible wave in the shallow water model is the gravity wave speed, C. At what y does the long Rossby wave speed equal the gravity wave speed? Again the answer is $y = \sqrt{C/\beta}$, and now with a very slim hint at an interpretation.

Given the (baroclinic) gravity wave speed, $C \approx 2.5$ m sec^{-1}, $R_{deq} = 340$ km. The local inertial period at that y is $2\pi/f = 4$ days. From this it appears that the eddy defined in the initial condition, radius L = 200 km, is small insofar as $L/R_{deq} \approx 1/2$ and it has been noted that the initial eddy was entirely dispersed into waves. The same result obtains even for a much larger eddy, $L = 500$ km, see
https://www2.whoi.edu/staff/jprice/eqtr-largeeddy

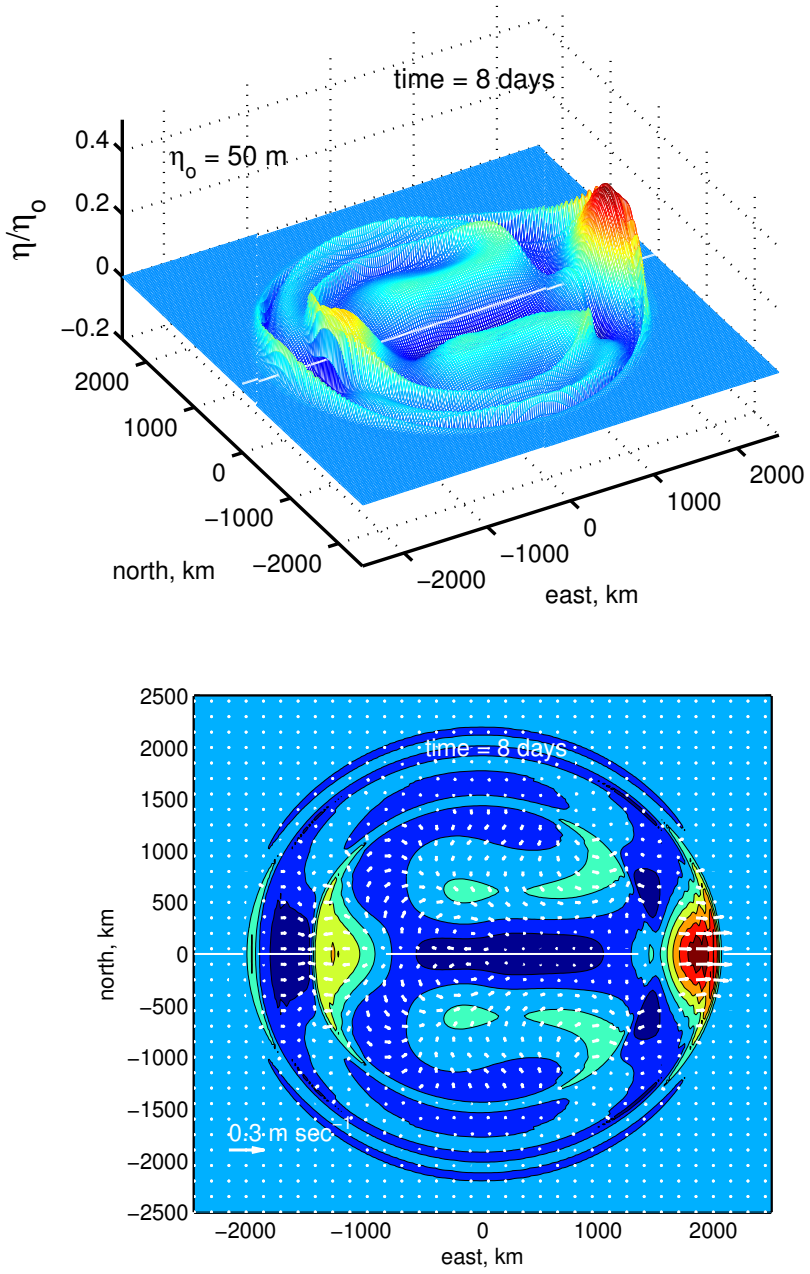

Figure 15: A snapshot from an equatorial adjustment experiment at time = 8 days after releasing a raised eddy centered on $(east, north) = (x, y) = (0, 0)$. The model domain extended 2500 km north and south of the equator (the thin white line), and sidewalls were placed at $x = \pm$ 2500 km. East is to the right. (The Pacific Ocean has more than three times this width.) **(upper)** The thickness anomaly, η. Notice that the largest feature is a positive bump centered on the equator and propagating eastward, evidently a Kelvin wave pulse as discussed in the main text. An animation of these data is eqtr-eta.mp4 in P3-videos. **(lower)** A plan view of the velocity, and color contours of η. Notice that velocity is generally normal to the η contours, indicating that these fields are mostly gravity wave motion. An animation of this data is eqtr-velocity.mp4

3.3 Dispersion relation of equatorially-trapped waves

Wave properties of the equatorial β-plane are clearly very important, and it wouldn't be exaggerating to say that waves of one kind or another are all that there is this adjustment experiment. For the purpose of examining wave properties it will be necessary to work with the linear shallow water system; substituting $f = \beta y$,

$$\frac{\partial h}{\partial t} \;=\; H(\frac{\partial u}{\partial x} \;+\; \frac{\partial v}{\partial y}), \tag{29}$$

$$\frac{\partial u}{\partial t} \;=\; -\,g'\frac{\partial h}{\partial x} \;+\; \beta y v, \tag{30}$$

$$\frac{\partial v}{\partial t} \;=\; -\,g'\frac{\partial h}{\partial y} \;-\beta y u. \tag{31}$$

Presuming the existence of zonally propagating waves that have an unknown y-dependence, then for the meridional velocity (this follows very closely the classic paper by Matsuno[17]);

$$v(x,y,t) \;=\; V(y)cos(kx_x - \omega t), \tag{32}$$

and similarly for $U(y)$ and $\Upsilon(y)$. By substitution into the linear shallow water equations and after eliminating $U(y)$ and $\Upsilon(y)$ by cross-differentiating and adding (as in the derivation of the potential vorticity balance) there results a second order, ordinary differential equation for $V(y)$,

$$\frac{d^2V}{dy^2} \;-\; \left(\frac{\beta^2y^2}{C^2} - \frac{\omega^2}{C^2} + \frac{\beta k_x}{\omega} + k^2\right) V \;=\; 0, \tag{33}$$

and a dispersion relation discussed below. To be physically realizable,

$$V(y) \rightarrow 0 \;\text{ as }\; \mid y \mid \;\rightarrow \infty. \tag{34}$$

Eqns. (33) and (34) have the form of a Shrodinger equation for a quantum harmonic oscillator, and the solutions are the set of eigenfunctions

$$V_n(y) = exp(-\frac{y^2}{2R_{deq}^2})H_n(\frac{y}{R_{deq}})$$

where H_n is the nth (physicist's) Hermite polynomial. The first five are $H_0 = 1$, $H_1 = 2y$, $H_3 = 4y^2 - 2$, and $H_4 = 8y^3 - 12y$. The eigenfunctions $V_n(y)$ are meridional normal modes that are numbered n = 0, 1, 2 etc. (Fig. 16, right). The Kelvin mode labeled $n = -1$ requires a separate discussion to follow. The eigenfunctions of the interface displacement, $\Upsilon_n(y)$, may be computed from the $V_n(y)$ as,[17]

$$\Upsilon_n(y) \;=\; 0.5(\omega R_{deq}/C - k_x R_{deq})V_{n+1}(y) \;-\; n(\omega R_{deq}/C + k_x R_{deq})V_{n-1}(y). \tag{35}$$

The odd numbered $\Upsilon_n(y)$ are symmetric about the equator, i.e., $\Upsilon_n(y) = \Upsilon_n(-y)$ (Fig. 16, right), while the even-numbered modes are anti-symmetric, $\Upsilon_n(y) = -\Upsilon_n(-y)$. This symmetry is very consequential for the excitation of the normal modes.

The dispersion relation $\omega(k)$ is

$$\omega^3 \; - \; \left(C^2 k_x^2 + \frac{(2n+1)C^2}{R_{deq}^2} \right) \omega \; - \; \beta C^2 k_x = 0, \tag{36}$$

where k is the zonal wavenumber (there is no north-south wavenumber by virtue of Eqn. 32), and n is the (meridional) mode number. This dispersion relation is cubic and so looks a bit complicated. However, its graph, Fig. (16, left) reveals two familiar wave types — higher frequency waves that are close analogs of the mid-latitude inertia-gravity waves, and lower frequency Rossby waves. As in the mid-latitude β-plane experiment, there is a significant frequency gap between the lowest frequency inertia-gravity wave, $\omega R_{deq}/C \approx 1.7$ (dimensional period = 5.4 days), and the highest frequency Rossby wave, $\omega R_{deq}/C \approx 0.3$ (period = 30 days).

The equatorial β-plane also supports two important wave types that are not found in the mid-latitude, open ocean. 1) The mode $n = 0$, appropriately called a mixed Rossby-gravity wave, has a $\omega(k)$ that closely parallels the Rossby wave modes for negative wave numbers (west-going waves), and parallels the inertia-gravity waves for positive wave numbers (east-going waves). The group speed of these waves is eastward at all frequencies. Depending upon the wavenumber, Rossby-gravity waves can have a frequency that is intermediate between the low frequency Rossby waves and the higher frequency inertia-gravity waves. Hence, there is no frequency gap in the family of free equatorial waves, as occurs at mid-latitudes. Unfortunately, these waves are not observed in the present experiment, because the mixed Rossby-gravity wave mode is anti-symmetric in $\eta(y)$ and so is not excited by the symmetric, initial thickness anomaly used here. 2) Second, the equatorial beta-plane also supports an eastward-going Kelvin wave, of which more below.

3.3.1 Westward-going gravity and Rossby waves

The most noteworthy wave motions appear to be trapped near the equator (Figs. 15 and 16). First, consider the wave motion(s) that are farthest west of the origin, $-2000 < x < -1800$ km, at time = 8 days. The velocity is almost normal to isolines of η and thus longitudinal and gravity wave-like. The meridional structure is a single maximum of meridional extent approx. R_{deq}, that is symmetric about the equator and thus meridional mode n = 1. The dominant wavelength is very roughly λ = 1000 km so that $kR_{deq} \approx 2$. In this $R_{deq}k_x$ range, the dispersion relationship for gravity waves is dispersive, and the group speed is slightly less than the maximum possible, $\sqrt{g'H}$. The $\eta(x)$ profile looks wave-like, vs. pulse-like

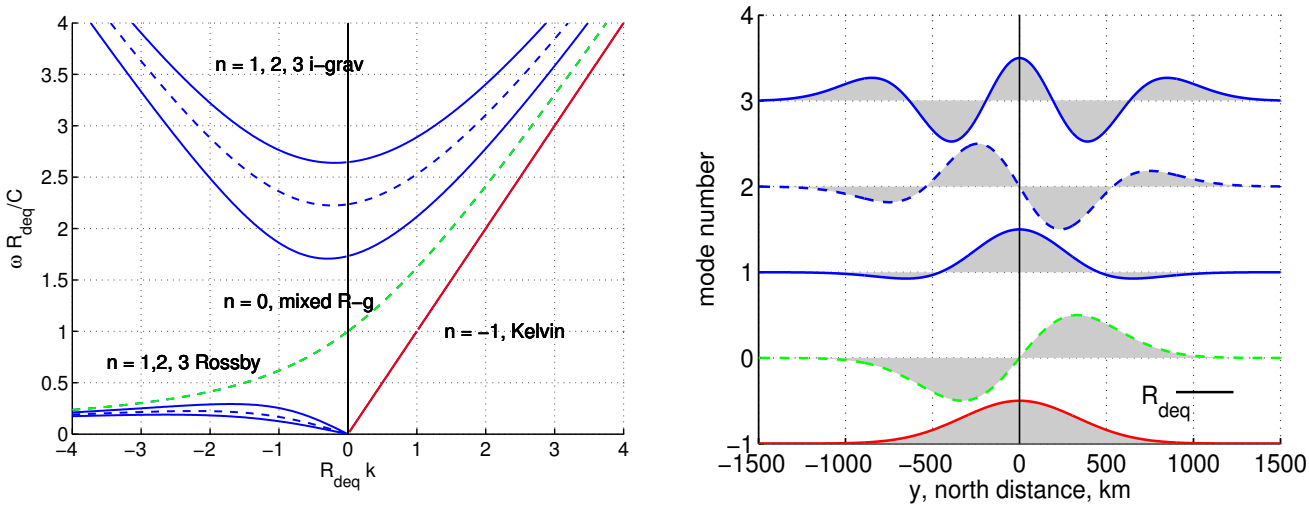

Figure 16: **(left)** Dispersion diagram for the trapped waves on an equatorial β-plane. The modes are numbered $n = -1, 0, 1...$ etc. The Kelvin wave $n = -1$ is in red, the mixed Rossby-gravity wave is in green dashed, and the inertia-gravity and Rossby waves are in blue. Modes that are symmetric in $\eta(y)$ are solid, while modes that are anti-symmetric are dashed. Note that the equatorial radius of deformation is used to nondimensionalize the zonal wavenumber, k_x, and the equatorial inertial period R_{deq}/C used to nondimensionalize the frequency. **(right)** The meridional modes of η, $\Upsilon_n(y)$, computed from the $V(y)$ modes and Eqn. (35) using $\omega R_{deq}/C \approx 2$ and $R_{deq}k_x \approx -1$, appropriate to westward propagating inertia-gravity waves. For Rossby wave values, the details are different, but the symmetry properties of the modes remain the same. The colors correspond to those at left, e.g., the Kelvin wave is in red. The amplitudes are arbitrary. Notice that lower numbered modes are effectively trapped near the equator, while higher modes may have an appreciable amplitude at higher latitudes.

(Figs. 17 and 18) Thus the leading, west-going waves appear to be equatorially-trapped gravity waves.

A somewhat larger amplitude westward-going feature trails behind the leading gravity waves; at time = 8 days a local maximum is centered on $(x, y) = (-1200, 0)$ km. The meridional structure is very similar to that noted above, mode $n = 1$, and Gaussian with north-south scale R_{deq}. The group speed is evidently about half or less of the fastest westward-going gravity waves noted just above. A qualitative difference with the gravity waves is that the velocity has some component along isolines of thickness, rather than normal as for gravity waves, and hence the velocity is somewhat geostrophic. These properties are consistent with a meridional mode 1 equatorial Rossby wave. Equatorial Rossby waves have a dispersion relation that is the low frequency limit of Eqn. (36),

$$\omega = -\frac{Ck_x}{R_{deq}^2 k_x^2 + (2n+1)}. \tag{37}$$

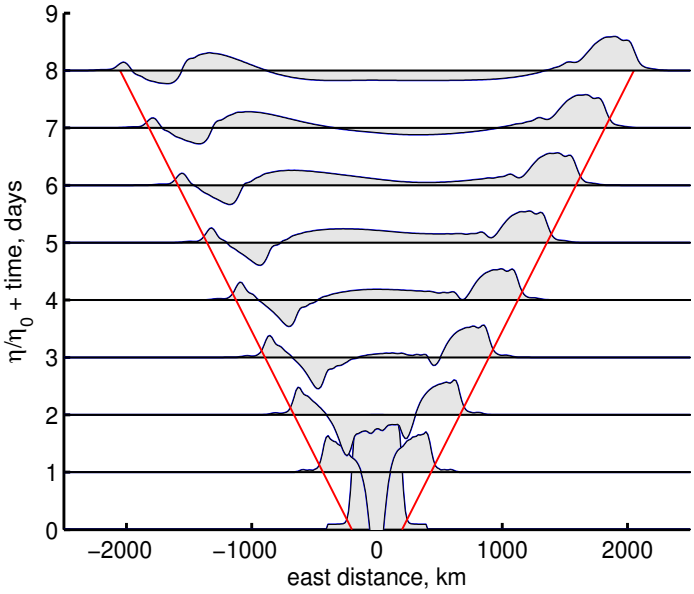

Figure 17: A series of slices through the numerical solution Fig. (15) along the equator showing $\eta(x, y = 0$,time = 0, 1, 2... days) normalized by $\frac{1}{2}\eta_0$. The red lines have a slope = $dx/dt = \pm C = \pm\sqrt{g'H}$. Notice that the westward-going, gravity wave packet changes shape with time and has only a small mean value. The eastward-going Kelvin wave pulse maintains a nearly constant shape and has an appreciable mean value. This illustrates the often qualitative difference between dispersive (westward-going) and nondispersive (eastward-going) wave propagation.

The long wave limit, $R_{deq}^2 k_x^2 \ll 1$, for $n = 1$ has phase and group speed

$$C_p = C_g = \frac{C\omega}{k_x} = -C/3$$

or about 100 km per day and westward. These long Rossby waves are nondispersive (although for the west-going waves considered as a whole there is clearly a significant range of phase and group speeds). It is notable that long equatorial Rossby waves have phase and group speed that are greater by a factor of about 30 than that of mid-latitude, long Rossby waves. This has great significance for the response of the equatorial ocean to seasonally varying wind stress, as we will discuss in Part 4.

3.3.2 Kelvin wave

The eastward-going motion is made up mainly of a very prominent isolated maxima in η that has the propagation properties of an equatorial Kelvin wave. This Kelvin wave pulse is important and interesting on two counts: first, it is the biggest feature in the solution, and second, it does not appear as a solution of the modal equation (33).

Suppose we did not know that this feature was a Kelvin wave — could we infer the dynamics from the properties evident in the numerical solution? Several useful clues are evident in a sequence of equatorial slices through the solution, Fig. (17), and in a magnified plan view, Fig. (18).

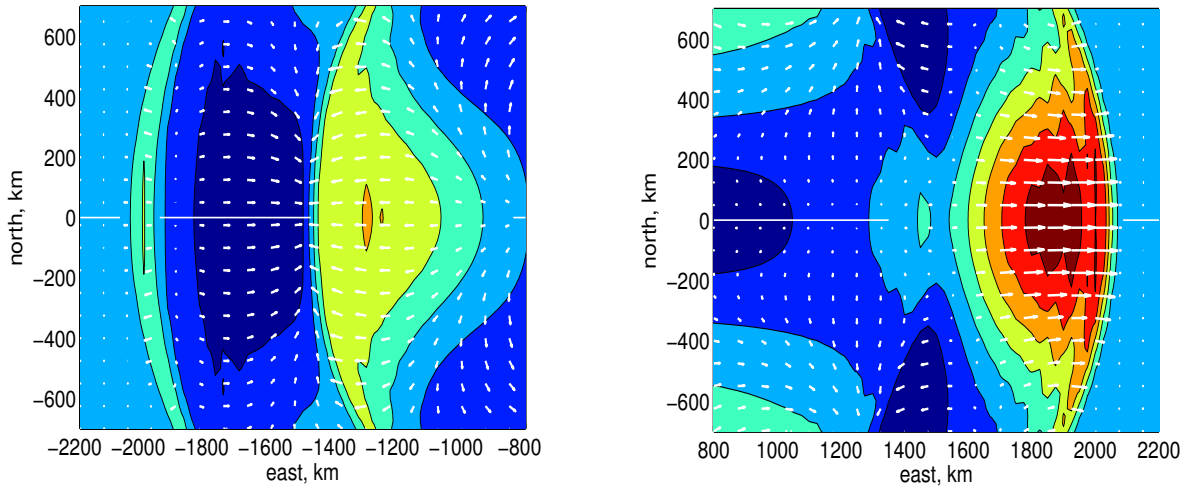

Figure 18: Enlarged snapshot views at time = 8 days of the equatorially-trapped, westward- and eastward-going local maxima from Fig. (15). **(left)** The westward-going pulse is dispersed into faster-moving gravity waves and slower moving, somewhat larger amplitude Rossby wave(s). Both kinds of westward propagating waves are evidently meridional mode 1 (Gaussian). **(right)** The eastward-going wave pulse has the properties of a Kelvin wave; the north-south structure is Gaussian, as at left, and the fluid velocity (the field of small white arrows) is directed almost exclusively east-west and

1. The pressure/velocity relationship is mainly longitudinal and the velocity is almost entirely zonal (east-west). Hence there is little or no β effect. These characteristics are consistent with a gravity wave, but not a Rossby wave.

2. Once this feature is separated from the initial eddy, the zonal wave form $\eta(x)$ remains almost constant as it propagates eastward at a speed very close to the gravity wave speed, $C = \sqrt{g'H}$. This is evidence of a nondispersive gravity wave motion as in Part 2, Sec. 3.1.

3. The meridional profile $\eta(y)$ is symmetric across the equator and is nearly self-similar, suggesting an equatorially-trapped wave mode. The half-width in y is about 400 km, or roughly R_{deq}.

The most telling/important clue to the dynamics is perhaps the first one, that $v = 0$. When this is implemented in the linear shallow water equations the result is a significantly reduced set:

$$\frac{\partial \eta}{\partial t} = H\frac{\partial u}{\partial x}, \tag{38}$$

$$\frac{\partial u}{\partial t} = -g'\frac{\partial \eta}{\partial x}, \tag{39}$$

$$0 \;=\; -g'\frac{\partial \eta}{\partial y} - \beta y u. \tag{40}$$

Eqns. (38) and (39) are exactly the pure gravity wave (nonrotating) system of Sec. 3.1 Part 2 and lead to the same elementary wave equation in (x,t);

$$\frac{\partial^2 \eta(x,y,t)}{\partial t^2} \;=\; g'H\frac{\partial^2 \eta(x,y,t)}{\partial x^2}, \tag{41}$$

and the familiar phase speed,

$$\frac{\omega}{k} \;=\; \sqrt{g'H} \;=\; C.$$

This phase speed does not depend upon k_x, and so this wave is nondispersive, which is consistent with the observed wave form Fig. (18). Eqn. (40) indicates a geostrophic balance for the east-west component of the velocity. Substitution of the updated Eqn. (32) into Eqn. (40) gives

$$0 \;=\; \frac{d\Upsilon(y)}{dy} \;-\; \frac{\beta\omega}{g'Hk_x} y\Upsilon(y). \tag{42}$$

Together with the boundedness requirement, this yields the $y-$dependence of the pulse shape, a Gaussian $\propto exp(-y^2/2R_{deq}^2)$, where $R_{deq} = \sqrt{C/\beta}$. Combining these two results gives a partial solution

$$\eta(x,y,t) \;=\; \eta_0(x)\exp\left(\frac{-y^2}{2R_{deq}^2}\right)\cos(k_x x - \omega t), \tag{43}$$

where $\eta_0(x)$ is the zonal width of the Kelvin wave pulse. The important qualitative results from this brief analysis are: 1) an equatorial Kelvin wave propagates eastward only, 2) it is non-dispersive, 3) it is symmetric across the equator (Fig. 16, right) and 4) it has a Gaussian zonal profile and zonal scale R_{deq}. The meridional profile is always the Gaussian of (43), regardless of the initial eddy size. However the width of the wave pulse, $\eta_0(x)$, is proportional to the width of the initial eddy, rather short in this experiment.

Because an equatorial Kelvin wave has zero meridional fluid velocity, it is not represented in the second order equation (33) for the meridional structure $V(y)$. Thus Eqn. (33) contains only a subset of the shallow water system, that having meridional velocity. The Kelvin wave has to be added to the solutions of Eqn. (33) in order to make a complete set and, more to the point, to account for the phenomenon seen in our numerical experiment. The Kelvin wave is usually assigned the label $n = -1$, since it's dispersion properties $\omega(k)$ fit Eqn. (36) for that n. Since there is no meridional flow across the equator, the equator could just as well be replaced by a (frictionless) wall insofar as the Kelvin wave alone is concerned.

The Kelvin wave is clearly a very important part of the adjustment process: inertia-gravity and

Rossby waves carry energy away from the collapsing eddy, but the Kelvin wave pulse carries energy along with roughly 2/3 of the excess layer thickness (initial eddy volume) towards the east. When the Kelvin wave pulse reaches the eastern boundary it is partially reflected back to the west in the form of equatorially-trapped inertia-gravity and Rossby waves. Most of the volume contained within the equatorial Kelvin wave is scattered onto boundary-trapped Kelvin waves that propagate north and south along the eastern boundary of the model domain (to see this you will need to view the animation linked in the caption to Fig. 15).[18]

3.4 Problems

(1) Some Kelvin wave questions for you. 1) In our geostrophic adjustment experiment the initial eddy had a positive η (easier to plot); suppose instead the initial eddy was a depression in the layer thickness; what differences might be expected for the Kelvin wave? Consider also finite amplitude effects that you can check with the numerical model. 2) Is it possible to have an equatorial Kelvin wave that propagates westward? 3) The zonal velocity of a Kelvin wave is in geostrophic balance with the tilted interface. Can you show that the resulting $u(y)$ is also consistent with one of the potential vorticity conservation modes discussed in Sec. 2.2.3, Part 2? 4) How would the Kelvin wave change if the initial eddy was made larger or smaller in the horizontal?

(2) The north-south symmetry of the initial condition chosen here had significant consequences for the waves that were generated during geostrophic adjustment. Suppose that the initial eddy was displaced off of the equator - what might be different? This is something you can check with a numerical experiment.

4 Summary and Remarks

This essay started with the question **What processes lead to the marked east-west asymmetry that is observed to characterize most large scale circulation (low frequency) phenomena?** Important examples of this asymmetry evident in Fig. (1) include the westward propagation of mesoscale eddies and the very marked westward intensification of the wind-driven gyres. This essay has emphasized the low frequency β-effect that arises from the northward variation of f combined with a balanced meridional velocity.

[18] An excellent online reference for the role of equatorial waves in the ENSO phenomenon is available at http://iri.columbia.edu/climate/ENSO/theory/index.html More on the equatorial Kelvin wave may be found at http://science.nasa.gov/science-news/science-at-nasa/2002/05mar_kelvinwave/ (you may have to type this in to your browser).

4.1 Mid-latitude mesoscale eddies

The first experiments considered in Sec. 2 included the geostrophic adjustment of a mesoscale-size thickness anomaly released onto a mid-latitude β-plane.

1) The short-term (several days) geostrophic adjustment process is little altered by β. The inertia-gravity waves that propagate poleward are, however, reflected when they reach a latitude where f is comparable to their intrinsic (initial) frequency. This βinduced reflection is an interesting and important process for inertia-gravity waves found in the open ocean, but it has no evident effect upon the adjusted eddy.

2) The long-term (weeks to months) evolution of a nearly balanced eddy includes β-induced westward propagation that is absent on an f-plane. For typical, subtropical C and f (30^o N) the eddy peak moves westward at about 3 km day^{-1}. The propagation speed increases sharply toward lower latitude. The numerical eddies studied here appear to make a good analog of oceanic mesoscale eddies (Fig. 1) insofar as they reproduce approximately the latitudinally-dependent zonal propagation of the eddies observed in SSH (problem 2.9.8). The β-effect acting upon nearly geostrophic eddies is a highly plausible mechanism for the observed, westward propagation of oceanic mesoscale eddies.

3) The β-plane shallow water system supports a low frequency wave, a planetary Rossby wave, that make a very useful analog of mesoscale eddies. Outside of the tropics, baroclinic, planetary Rossby waves have a low frequency, typically only about one percent of f, and currents that are nearly geostrophic. Rossby waves are markedly anisotropic in that they propagate phase westward only. Elementary (plane) Rossby waves are not commonly observed in the ocean or atmosphere but they are of great interest here because they have time and space scales in common with mesoscale eddies, and long baroclinic Rossby waves exhibit a very similar potential vorticity balance, β balanced by stretching. The phase and group speed of long, nondispersive Rossby waves is $-\beta/R_d^2$ (westward), which is just slightly greater than the propagation speed of the numerical mesoscale eddies, including the marked latitudinal dependence.

4) Insofar as westward propagation alone is concerned, the numerical eddies look to be an essentially linear phenomenon. However, their amplitude measured by thickness anomaly is appreciable, $\delta h/H \approx 0.1$, and their typical currents are several times greater than their propagation speed. As a consequence, they are likely able to trap and transport tracer for an appreciable distance. Insofar as transport goes, the numerical eddies exhibit important finite amplitude effects.

4.2 Equatorial Adjustment

5) The equatorial region — aside from the western boundary — appears to be almost free of mesoscale eddy variability ($L \propto$ several hundred km).[19] An adjustment experiment set up in an equatorial ocean suggests one reason for this may be that anomalies with horizontal scales $L < 500$ km will disperse into gravity and Rossby waves before adjusting to geostrophy. This is an extension of the main result from Sec. 4 Part 2 that the fraction of an initial anomaly that survives geostrophic adjustment is dependent upon the ratio L/R_{deq}, where the equatorial radius of deformation is $R_{deq} = \sqrt{C/\beta} = 250$ km and about five times greater than the mid-latitude equivalent.

6) Eastward propagation of a Kelvin wave is the most prominent feature of the equatorial adjustment experiments studies here (in part due to the symmetric initial condition) and is an occasional and sometimes very prominent feature also of the real equatorial oceans. The Kelvin wave has phase and group speed equal to the gravity wave speed, and is nondispersive. A Kelvin wave that is generated in mid-ocean (say by a rapid change in the winds) will thus reach the eastern boundary in a matter of weeks. There it is scattered into boundary Kelvin waves that propagate north and south along the eastern boundary of both hemispheres, and to a lesser extent, into westward traveling, dispersive, equatorially-trapped gravity and Rossby waves.

7) The equatorial ocean differs from the midlatitude beta-plane ocean in that the frequency gap between inertia-gravity waves and Rossby waves is much smaller; the inertia-gravity waves have a comparatively low (dimensional) frequency, and the Rossby waves a comparatively high frequency and fast group speed. As we will see in Part 4, this has the consequence that the equatorial and topical oceans adjust comparatively very rapidly to wind stress, including annual variations.

4.3 Remarks

An important result implicit in 1) above is that a mid-latitude β-plane supports two distinctly different, and for the most part non-interacting kinds of waves and associated dynamics: fast time-scale inertia-gravity waves and slow time-scale, quasi-geostrophic Rossby waves and eddies. This has practical importance on several levels. Insofar as westward propagation of midlatitude mesoscale eddies is concerned, it would have been simpler to start the experiment with a balanced eddy and forego the geostrophic adjustment and inertia-gravity waves. There is a pedagogic aspect as well. It is sensible to

[19] Mesoscale eddy-like features do appear seasonally some years, in especially the North Pacific equatorial ocean. These eddies are thought to result from an instability of the wind-driven equatorial current system and are termed Tropical Instability Waves. An excellent, brief introduction is http://en.wikipedia.org/wiki/Tropical_instability_waves

introduce geostrophic adjustment and Rossby wave dynamics as separate topics, rather than conflate them as they have been here. The rationale for considering these phenomenon in the same experiment is partly that the clear separation of time scales and dynamics that characterizes mid-latitudes does not extend to the equatorial region where inertia-gravity waves and Rossby waves have overlapping time and space scales.

The present numerical experiments start from a highly idealized initial condition, a right cylinder of thickness anomaly having a specified radius and that is released into a still ocean. The sudden release of this anomaly produces a fairly broad wavenumber and frequency spectrum, including gravity waves and short Rossby waves having eastward (but very small) group speed. This is not realistic of actual oceanic mesoscale eddies that are formed from a comparatively slowly growing instability of larger-scale, nearly geostrophic currents, e.g., a Rossby wave Sec. 2.7, and so are close to geostrophic balance from the outset. A fairly crude representation of this follows form initializing an adjustment experiment with a very large eddy, say radius $L = 1000$ km, or more to the point, $L = 20R_d$. The central portion of this eddy remains flat and at rest after the edges have adjusted to geostrophy. The subsequent evolution of this eddy is quite different from the propagation of a long Rossby wave, and neither is it anything like a small, wind-driven gyre. The southerly flow along the western edge of the initial (large) eddy is unstable and spontaneously forms smaller eddies having a diameter of about 300 km. These eddies are very similar to the eddies made here by geostrophic adjustment from a state of rest, although a little larger. This eddy formation process likely has some important elements in common with the formation of real oceanic mesoscale eddies, though this particular experiment lacks adequate vertical resolution.

In regions having intense currents, e.g., the Gulf Stream and extension of Fig. 1, the ocean is teeming with mesoscale eddies, that are not isolated from one another in a homogeneous environment as presumed here. As well, there are other kinds of oceanic variability and of course, sea floor topography. Interactions between neighboring eddies and between eddies and the atmosphere give rise to phenomena that modify the eddies and the larger scale environment significantly.[20]

4.4 What's next?

Part 4 will study basin scale, wind-driven flow using the same shallow water model used here, but augmented with a body force that mimics wind stress and boundary conditions that define a closed basin. The aim will be to elucidate the mechanism(s) that lead to western intensification of the major ocean

[20]McGillicuddy, D., et al., 'Eddy/wind interactions stimulate extraordinary mid-ocean plankton blooms', *Science*, 316, 1021 (2007), DOI: 10.1126/science.1136256 See also Chelton, D. B., P. Gaube, M. G. Schlax, J. J. Early and R. M. Samelson, 'The influence of nonlinear mesoscale eddies on near-surface oceanic cholorphyll', *Science*, 334, 21 Oct 2011, 328-332, doi: 10.1126/science.1208897

gyres. It will become clear that eddies and gyres are close cousins in that they share the beta-effect. In the case of eddies, the beta effect is balanced by time dependence; in the case of the wind-driven gyres, the beta effect is balanced the divergence of Ekman transport associated with wind stress curl. The final, Part 5, studies the very interesting response of the Arabian Sea to the South Asia Monsoon winds.

Index

Resource: Topics in Fluid Dynamics

James Price